PREPRINT

tascc

TASCC-P-96-30

FORMATION OF AN INTERMEDIATE-VELOCITY REMNANT IN $^{35}Cl + ^{12}C$, ^{24}Mg AND ^{197}Au REACTIONS AT 43 MeV/NUCLEON

Y. Larochelle, L. Gingras, L. Beaulieu, X. Qian, Z. Saddiki, B. Djerroud*, D. Doré†, R. Laforest‡, R. Roy, M. Samri and C. St-Pierre
Laboratoire de physique nucléaire, Département de physique, Université Laval, Québec G1K 7P4, Canada

J.A. López and T.Robinson
Department of Physics, University of Texas at El Paso, El Paso, TX 79968-0515,USA

G.C. Ball, D.R. Bowman, A. Galindo-Uribarri, E. Hagberg and D. Horn
AECL, Chalk River Laboratories, Chalk River, ON K0J 1J0, Canada

* *Present address: NSRL, University of Rochester, 271 East River Road, New York 14627, USA*
† *Present address: Institut de Physique Nucléaire d'Orsay, B.P. 91406, Orsay Cedex, France,*
‡ *Present address: AECL, Chalk River Laboratories, Ontario K0J 1J0, Canada*

Submitted to
Phys. Rev. C

Physical and Environmental Sciences
Chalk River Laboratories
Chalk River, ON K0J 1J0 Canada

1996 August

Formation of an intermediate-velocity remnant in $^{35}Cl + {}^{12}C$, ^{24}Mg and ^{197}Au reactions at 43 MeV/nucleon

Y. Larochelle, L. Gingras, L. Beaulieu, X. Qian, Z. Saddiki, B. Djerroud *, D. Doré †, R. Laforest ‡, R. Roy, M. Samri and C. St-Pierre

Laboratoire de physique nucléaire, Département de physique, Université Laval, Québec, Canada G1K 7P4

J.A. López and T. Robinson

Department of Physics, University of Texas at El Paso, El Paso, TX 79968-0515, USA

G.C. Ball, D.R. Bowman, A. Galindo-Uribarri, E. Hagberg and D. Horn

AECL, Chalk River Laboratories, Ontario, Canada K0J 1J0

(August 27, 1996)

*Present address: NSRL, University of Rochester, 271 East River Road, New York 14627, USA

†Present address: Institut de Physique Nucléaire d'Orsay, B.P. 91406, Orsay Cedex, France

‡Present address: AECL, Chalk River Laboratories, Ontario, Canada K0J 1J0

Abstract

The experimental signature of the formation of an intermediate-velocity remnant, with a velocity between that of the projectile-like emitter and that of the target-like emitter, is investigated with the same beam and experimental setup for targets lighter than, comparable to, and heavier than the projectile. Experimental evidence for the dynamical production of intermediate mass fragments (IMF) and light charged particles from such a remnant is presented for the three reactions, $^{35}Cl + ^{12}C$, ^{24}Mg and ^{197}Au at 43 MeV/nucleon. Particle velocity distributions are compared with filtered 1- and 2-source statistical simulations. The production of IMF from the intermediate-velocity remnant occurs in less than 40% of the detected events, representing an estimated 10% of the reaction cross section. In the second part of the paper, different dynamical and phenomenological models are discussed and their predictions are compared to the experimental results. In particular, dynamical model simulations for the $^{35}Cl + ^{12}C$ system with the formation of an intermediate-velocity remnant are presented. Finally some hypotheses for the reaction mechanism leading to the formation of an intermediate-velocity remnant are discussed.

PACS number(s): 25.70.Mn, 25.70.Pq

I. INTRODUCTION

There is strong evidence that reaction dynamics play an important role in the multi-fragmentation process of heavy ions at intermediate energy [1–9]. In particular, persistence of final-state configurations having a binary character well into the Fermi energy range (10 MeV/nucleon< E_{beam} <100 MeV/nucleon), even for very central or violent collisions, has been confirmed in several recent experiments [10–15]. However, this penomenon still evades proper theoretical explanation. It has been shown that for reactions involving light heavy ions (Z<20), the fusion cross section is only 4% or less [14,15] of the total reaction cross section. Another observed phenomenon, still not well understood, is the formation of a neck-like structure, recently evidenced in reactions between very heavy ions [16–18] in the Fermi energy range. The concept of a "neck" in configuration space between the projectile and the target might be related to the velocity space concepts of mid-rapidity source, participant-spectator phenomena or "fireball" models commonly used for higher-energy heavy-ion reactions [19–23]. In a study of the Kr + Au reaction at 43 MeV/nucleon, Stuttgé at al. [24] concluded, based on velocity distributions, that intermediate-velocity fragments ($Z \geq 9$) might come from a participant zone.

In this paper we present experimental evidence for the formation of an intermediate-velocity remnant, probably through a dynamical process, dissociated from the projectile-like and target-like emitters and responsible in part for intermediate-mass fragment (IMF, here defined as $3 \leq Z \leq 9$) production in the Fermi energy range. Three different targets (^{12}C, ^{24}Mg and ^{197}Au) have been used with a ^{35}Cl projectiles at 43 MeV/nucleon in order to assess the similarities between nearly symmetric and very asymmetric systems. In the three cases, noticeable differences have been observed between the experimental results and simulations of the statistical decay of two-source systems.

The second half of the paper discusses possible theoretical explanations for the formation of an intermediate-velocity remnant for the systems studied. Dynamical models such as Boltzmann-Uehling-Uhlenbeck (BUU) [25] and Quantum Molecular Dynamics (QMD) [6,26]

are briefly introduced and simulations for the $^{35}Cl + ^{12}C$ system presented. Although the formation of an intermediate-velocity remnant from dynamical fluctuations is predicted by the QMD model, this process has a very low cross section and most collisions result in compound nucleus formation or deep-inelastic binary systems.

Another interesting model developed in recent years is the alpha-cluster molecular dynamics model of Möhring et al. [27]. Although it should be compatible with our small $A/Z \approx 2$ systems, it failed to reproduce the dissipative binary dynamics and intermediate-velocity remnant formation observed experimentally for mid-peripheral or central reactions. A different approach to alpha-cluster molecular dynamics is also briefly presented in this section.

The low-energy di-nuclear orbiting model [28–34] is reviewed and the possibility of the formation of a third source is assessed. Nuclear transparency (nucleon mean-free path) in a Fermi gas is discussed along with its implication for binary mechanisms. Finally recent results on hollow configurations in expanding nuclear matter by Borunda and Lopez [35] are presented. This last approach could give some insights on the origin of the dissipative binary collision mechanism and the formation of an intermediate-velocity remnant.

II. EXPERIMENTAL SETUP

The experiment was performed at the Tandem Accelerator SuperConducting Cyclotron (TASCC) at Chalk River. A beam of ^{35}Cl at 43 MeV/nucleon bombarded successively a 2.2 mg/cm^2 thick carbon target, a 1.9 mg/cm^2 magnesium target and a 2.9 mg/cm^2 gold target. The reaction products were detected in an array of 83 detectors covering polar angles from 3.0° to 46.8°. The 80 detectors of the Laval-Chalk River forward array [37,38] are mounted in five concentric rings around the beam axis and cover nearly 100% of the solid angle between 6.8° and 46.8° (see fig. 1). The first three rings are made of plastic phoswich detectors with a detection threshold of 7.5 (22.5) MeV/nucleon for Z=1 (17) particles. The two outer rings are composed of CsI(Tl) crystals which achieve isotopic resolution for Z=1 and 2 ions with a threshold of 2 MeV/nucleon and element identification for Z=3 and 4 ions with a threshold of 5 MeV/nucleon. For the ^{35}Cl + ^{24}Mg experiment, three Si-CsI telescopes sampled the most forward angles, 3.0° to 5.0°, and provided charge identification with a detection threshold of 2 (5) MeV/nucleon for Z=2 (17) particles. More details on the experimental setup can be found in ref. [9,15,36]. Between 10^5 and 10^6 events were recorded for each projectile-target combination in both "minimum-bias" and central triggering conditions (charged-particle multiplicities $\geq$ 2 and $\geq$ 6, respectively).

Since the effects of the detectors' energy thresholds are different on each system, because of the different system sizes and center-of-mass (c.m.) velocities, a careful selection of events for each experiment must be made before investigating the formation of an intermediate-velocity remnant. Figure 2 shows the c.m. velocity, reconstructed from all detected particles, of the events considered in the present analysis. For the lightest system, ^{35}Cl + ^{12}C, 2×10^5 completely detected events (ΣZ=23) are retained. The reconstructed c.m. velocity of the system is narrow and centered at the calculated value. For the nearly symmetric system, ^{35}Cl + ^{24}Mg, completely detected events (ΣZ=29) represent only a small fraction of the data, mainly because the phoswich detectors' threshold is closer to the c.m. velocity. All events with at least 80% or more of the charge ($\Sigma Z \geq 23$) detected were included in the analysis.

For this system, the reconstructed c.m. velocity is still close to the entrance channel c.m. velocity, but slightly shifted toward the beam velocity, showing that the missing charges are emitted at backward c.m. angles. In the case of the asymmetric system $^{35}Cl + ^{197}Au$, the array threshold limits contribution from the target to a few light charged particles (LCP), and the reconstructed c.m. velocity for events with minimum bias ($15 \leq \Sigma Z \leq 20$) is very close to the beam velocity. A contribution from the quasi-elastic scattering of the projectile can be observed at the beam velocity (9.12 cm/ns). However, as shown in section II.B, experimental bias does not exclude the detection of LCP and light IMF (Z=3,4) from a neck-like structure for this system.

III. RESULTS AND ANALYSIS

A. The $^{35}Cl+^{12}C$, $^{35}Cl+^{24}Mg$ experiments

The formation of a remnant in an intermediate energy heavy-ion reaction should not necessarly be considered as the appearance of a new "emitting source" in the system. Rather it can be thought of as a hot remnant likely produced via both direct nucleon-nucleon interaction and collective mean-field behaviour occurring near the c.m. velocity of the system. The presence of such an intermediate-velocity remnant in a reaction would mean that this is a "ternary" event, where reaction products have three different possible origins: the projectile-like emitter (PLE), the target-like emitter (TLE) and the intermediate-velocity remnant. The persistence of the dissipative binary character in the Fermi range and the formation of an intermediate-velocity remnant at c.m. velocity are signs that the incomplete fusion mechanism [39–47] is likely in competition with a dynamical mechanism for the production of IMF.

To extract an experimental signature from an intermediate-velocity remnant, one must first account for the experimental bias of the data. The c.m. velocities of the systems are 6.8 cm/ns for $^{35}Cl+^{12}C$ and 5.4 cm/ns for $^{35}Cl+^{24}Mg$, close to the forward array phoswich thresholds of 5.1 (6.3) cm/ns for Z=6 (Z=12). Because the energy threshold increases with particle charge, detected heavier fragments are likely to be faster on average than lighter ones. In order to properly assess threshold effects and to avoid experimental artifacts, every experimental distribution will be compared to simulations from the code EUGENE [48], filtered for both the detector's energy threshold and geometry. This code produces two-source events that are realistic in kinematics, excitation energy (equal temperature limit approximation) and angular momentum sharing between the nuclei. Complete fusion is predicted for small impact parameters, allowing the treatment of single- and two-source simulations with the same code.

As shown in ref. [14,15] for light systems, a small portion of the reaction cross section

in this energy range leads to single-source events. It is important to separate those events from the data before making a comparison to binary simulations. To do so an event-shape tensor analysis was performed using the quadratic momentum tensor [49]:

$$P^2_{i,j} = \Sigma_{n=1}^{N_{CP}} P_i^{(n)} P_j^{(n)}; i,j = 1,2,3 \quad (1)$$

where $P_i^{(n)}$, $P_j^{(n)}$ are the ith or jth Cartesian c.m. components of the particle momentum and N_{cp} is the total number of charged particles in the event. The three eigenvalues and eigenvectors calculated from this tensor define the shape of the event. The angle between the major axis of the event in momentum space (the eigenvector with the largest eigenvalue) and the beam axis is Θ_{flow}, the flow angle.

Figure 3 shows the experimental flow angle distributions for the two systems and corresponding simulations. Based on perpendicular versus parallel velocity spectra, it has been demonstrated in ref. [15] that a cut on the flow angle is a better criterion than transverse energy for isolating binary (or ternary) events. Furthermore, distributions of flow angle for single-source events plotted in the figure show that a majority of these events do correspond to the highest values of Θ_{flow}. The Z=3 perpendicular versus parallel velocity spectra for specific ranges of the flow angle are shown in fig. 4 for ^{35}Cl + ^{12}C, where the cut for binary (or ternary) is set at $\Theta_{flow} \leq 65^o$ and in fig. 5 for ^{35}Cl + ^{24}Mg, where the cut for binary (or ternary) is set at $\Theta_{flow} \leq 50^o$. It is clear from the velocity maps that the two-source events are selected by this cut on Θ_{flow} and single-source events, where the IMF emission is isotropic in the center of mass, are largely eliminated. The single-source events thus eliminated from the analysis for both systems represent 10% or less of the total yield.

As in previous analyses [9,13,15], the anisotropy ratio [50] is used to compare data and simulations that have the same elongation in the momentum space. This anisotropy ratio is defined as

$$R_A = \frac{2}{\pi} \frac{\sum_{i=1}^{M} |P_{ic.m.\perp}|}{\sum_{i=1}^{M} |P_{ic.m.\parallel}|}, \quad (2)$$

where $\frac{2}{\pi}$ is a geometric normalisation constant, M is the charged-particle multiplicity, and $P_{ic.m.\parallel}$, $P_{ic.m.\perp}$ are momenta of the i^{th} particle in the c.m. frame, parallel and perpendicular

to the beam axis. Figure 6 shows that in order to reproduce the anisotropy distribution of the ΣZ=23 data in ^{35}Cl + ^{12}C, EUGENE simulations of two-source events with an impact parameter of 4.0 fm or greater are required. For events with $\Sigma Z \geq 23$ detected in ^{35}Cl + ^{24}Mg, the value used in the simulations is 3.8 fm. Single-source events have on the average a mean value of anisotropy ratio higher than that of the data.

To properly assess the difference between binary and ternary events, we inspect the particle velocity distributions. Figure 7 shows perpendicular versus parallel velocity for LCP in the ^{35}Cl + ^{12}C c.m. system with Θ_{flow} <45° (corresponding to the events where the sources are very well separated) and ^{35}Cl + ^{24}Mg system with Θ_{flow} <30°. These cuts on Θ_{flow} are used for the remainder of the analysis. As previously, velocity maps are shown where the parallel axis is the beam axis (left side) or the major axis of the event (right side). Because of the large velocity range of such particles, it is difficult to isolate the sources of emission. Another difficulty with LCP is the pre-thermalization emission (for example, see refs. [39,46,51–54]), which further blurs identification of their point of origin. For these reasons our source analysis focuses on IMF.

Figure 8 is a similar plot of the c.m. velocity distributions for ions of Z=4 to 6 in the ^{35}Cl + ^{12}C system with Θ_{flow} <45° and the ^{35}Cl + ^{24}Mg system with Θ_{flow} <30°. A small range of IMF charge was chosen in order to eliminate bias induced by the Z-dependent energy thresholds for different detectors. The distribution in velocity space shows the presence of IMF from both the PLE at high parallel velocity, and the TLE (in the CsI(Tl) rings). There is also an important contribution at c.m. velocity, that is not related to either emitter. This is especially apparent from the spectra with the major axis as the parallel axis, but also on the left side where the detector energy thresholds are clearly outlined.

In order to find the kinematic origin of the particles emitted during the reaction, an exclusive analysis is performed based on the heaviest fragments of each event. Results from filtered EUGENE two-source simulations indicate that detected fragments originating from the TLE are mostly found in CsI(Tl) detectors (between 24° and 47° in the laboratory). Most of those coming from the PLE are found in the plastic phoswich array and Si-CsI telescopes

(together covering angles between 3° and 24°). Based on these results, the following method is used to probe the emission sources: the two forward heaviest fragments (detected in phoswiches or telescopes) and the backward heaviest one (detected in CsI(Tl)) were identified for each event. Individual and total velocity distributions of these three groups of fragments are presented in fig. 9 for the $^{35}Cl + ^{12}C$ system. Since an intermediate-velocity remnant would be better characterized kinematically by the presence of an IMF, only these particles ($3 \leq Z \leq 9$) are plotted in this figure. It should be observed that the forward heaviest fragment travels with an average velocity of 2.3 cm/ns (in c.m. reference frame). There are two major contributions of the second-heaviest forward fragment, found close to the heaviest and near the c.m. velocity (-1.5 cm/ns). The backward heaviest fragment has an average velocity of -4 cm/ns.

Because the phoswich energy threshold increases with the charge, the second observed heaviest fragment is often slower. For a better evaluation of bias, two-source simulations are analysed in the same way for comparison. Figure 10 shows the same velocity distributions as fig. 9, but for the filtered $^{35}Cl + ^{12}C$ EUGENE two-source simulation. Here, the average velocity of the forward heaviest fragment is estimated at 1.6 cm/ns. This is a lower value than the 2.3 cm/ns of the data, even though the momentum anisotropy of the data is well reproduced by the simulations, as shown in fig. 6. Also, there is no depletion between the heaviest and second heaviest fragments. These differences with data could be explained by the presence of a faster and lighter PLE in the data and the formation of an intermediate-velocity remnant travelling near the c.m. velocity.

Figure 11 and 12 show velocity spectra, from experimental data and EUGENE filtered simulations respectively, obtained with the same procedure as previuosly, but for the $^{35}Cl + ^{24}Mg$ system. Here again three sources can be identified on the experimental plot (fig. 11): The PLE, TLE and intermediate-velocity remnant with c.m. frame velocities of 3, -3 and 0 cm/ns respectively. Again, EUGENE simulations (fig. 12) do not reproduce the ternary nature of the data.

It is interesting to compare the three source velocities extracted from the IMF to the LCP

velocity map of fig. 7. Remarkably there is no important contribution from light particles above 3 cm/ns where the heaviest fragment, corresponding to the PLE, has been observed. Also there are LCP's just below the c.m. velocity where the IMF count is very low, because of the phoswich threshold. These LCP emission characteristics could be explained by the fact that the PLE did not gain much excitation energy during the collision, rather acting as a "spectator". The intermediate-velocity emission probably also contributes to the LCP intermediate velocity spectra. Recently, in a similar system, for a slightly higher energy range (^{36}Ar + ^{27}Al from 55 to 95 MeV/nucleon), Péter et al. [14] observed a pre-thermalization source at mid-rapidity contributing to the LCP velocity maps.

From the velocity observables, the assumption can be made that the intermediate-velocity remnant is a moderately excited residue of a dynamical process, and as such a source of LCP's. Based on the flow angle (Θ_{flow}) cuts made for the velocity maps, the presence of an intermediate-velocity remnant can be observed in a maximum of 40% of the detected events for the ^{35}Cl + ^{24}Mg system, and 50% for the ^{35}Cl + ^{12}C system. These percentages are upper limits since there is a condition on the total detected charge for both experiments, and since the identification of the intermediate-velocity remnant was not made on an event-by-event basis. To obtain a rough estimate of the cross section for dynamical IMF production (assuming no more than one intermediate-velocity IMF per event) for the ^{35}Cl + ^{24}Mg system, the number of IMF in frame b) of the fig. 11 related to an intermediate-velocity fragment remnant was evaluated. The number of IMF in that frame corresponds to 20% of the total number of all detected events, without selection on the flow angle. Because of the suppression of small angles in the experimental setup, and based on calculations in ref. [15], the actual cross section for the process can be estimated to be half that amount, or about 10% of the total cross section.

The contribution of intermediate-velocity IMF from one-source events should be negligible because of the cut on Θ_{flow}. From the filtered 1-source EUGENE simulations, we know that the flow angle distribution is approximately sinusoidal (see fig. 3). By comparing to the experimental distribution, the contribution of 1-source events to the intermediate-velocity

IMF map can be estimated to less than 1% of detected events with the cuts on the flow angle for both systems.

B. The $^{35}Cl+^{197}Au$ experiment

For an asymmetric collision of a light projectile with a heavy target, the analysis must be done differently, mainly because the energy threshold of the experimental apparatus only permits the detection of projectile residues and of fast light particles from the target. While the formation of an intermediate-velocity remnant in such an asymmetric system has never been observed directly, the signature of intermediate-velocity emission in low-Z energy spectra at large angles and "quasi-free nucleon knock-out" at more forward angles has been presented by Awes et al. [55] for the ^{16}O +Au system. This model failed to reproduce data for a more symmetric system. Even with threshold-less detectors, the kinematics involved in a very asymmetric collision makes it difficult to select particles emitted from an intermediate-velocity remnant since the c.m. velocity of the system would be extremely close to the target velocity. However, the intermediate-velocity source identified in asymmetric collisions was often found to be close to half the projectile velocity [7], even in the intermediate energy range of our experiment [56], leading to the conclusion that this intermediate system could be formed by nucleon-nucleon scattering between the projectile and the target [57].

For the analysis of the $^{35}Cl+^{197}Au$ reaction at 43A MeV, the code GENEVE [58] was used for comparison with the data instead of EUGENE. It also evaluates the early stage of the reaction with respect to excitation energy sharing and angular momentum, but it has provisions to include projectile-like and target-like preequilibrium emission of protons and neutrons. In the dissipation stage, at small impact parameters, the code assumes a complete damping of the initial relative motion between the two nuclei and the formation of a thermalized compound nucleus (incomplete fusion). For larger impact parameters, the excitation energy is shared between the PLE and the TLE, according to their relative masses. The deexcitation phase is similar to that followed by the code EUGENE. Simulations leading

to incomplete fusion were not retained for the present analysis.

In fig. 13, the distributions of velocity parallel to the beam in the laboratory reference frame for particles with Z=1,2,3 and 4 is compared to filtered GENEVE projectile break-up simulations. For both the data and the simulations the only event selection criterion has been that at least 15 charges were detected and that one fast heavy fragment (Z>5), corresponding to the PLE evaporation residue, was detected in the phoswich forward array. The main characteristic of the spectra is the "shoulder" present in the data below the main peak of the distributions seen above the detector threshold and absent in the simulations. The thresholds in the simulations are lower than for the data because they take into account only the detection threshold but not the additional threshold imposed by charge identification gating. These "shoulders" in the lower part of the light-particle and IMF velocity spectra were observed in other projectile break-up analysis done with completely different experimental setups [59,60], and were not attributed as a contribution from the heavy target. Also interesting is the difference between the experimental peak position and that of binary simulations. The experimental maximum is at a systematically higher velocity, especially for the heavier Z=3 and Z=4 particles, indicating a faster velocity for the PLE. The same trend had been observed for the lighter nearly-symmetric system detailed in the last section. Nucleon-nucleon scattering at mid-rapidity could produce LCP at the c.m. velocity, but not the heavier fragments. On the other hand, the trend in the data is compatible with the formation of an intermediate-velocity remnant, resulting in a greater kinematic separation between the PLE and TLE, or in this case the light PLE and the heavy target.

To further explore the effects of detector bias and the contribution from the target and/or preequilibrium emission to the velocity spectra, fig. 14 shows the filtered GENEVE Z=1 parallel velocity distribution and the relative contribution from the PLE (top panel), TLE (middle panel) and projectile-like preequilibrium (bottom panel). From these plots, it can be concluded that the experimentally observed shoulders do not arise from either TLE or from preequilibrium LCP emission, which is centered on the PLE velocity. This represents additional evidence of the formation of an intermediate-velocity remnant, or possibly a

neck-like structure due to the neutron-rich nature of the heavy target in the asymmetric $^{35}Cl+^{197}Au$ reaction.

This effect is even stronger when looking at isotopic ratios outside the normal emission range of the PLE. Based on systematics put forward by Lleres et al. [61] to isolate the PLE, the emission range of an excited ^{35}Cl is set at +/- 4cm/ns around the PLE residue. Figure 15 shows the proton, deuteron and triton ratios to the corresponding total number of hydrogens for parallel velocities lower and higher than 4 cm/ns to that of the heavy PLE residue. The ratio distribution for forward emission is well reproduced by GENEVE simulations. However, although there is a small change in the simulation, the backward ratios are dramatically different for the experimental data, showing many more neutron-rich deuterons and tritons. This is further evidence for the formation of an intermediate-velocity remnant (or neck-like structure), richer in neutrons than the PLE because of a contribution to its composition from the neutron-rich target.

IV. REACTION MECHANISM HYPOTHESES

Statistical codes such as EUGENE and GENEVE (and the combinations of TORINO [62] with GEMINI [63] or SOS [64] as used in refs. [9,13]) are based on excitation mechanisms involving nucleon exchange or excitation energy sharing as a function of the impact parameter, and on sequential evaporation of a statistical nature. Moreover, they do not predict the formation of an intermediate-velocity remnant, as shown in the previous section. In this section, we analyze different dynamical calculations and reaction mechanism scenarios which could shed some light on the experimental results, especially on the persistence of binary dynamics and the formation of an intermediate-velocity remnant.

A. Dynamical Models: BUU and QMD

Boltzmann-Uehling-Uhlenbeck (BUU) and Quantum Molecular Dynamics (QMD) models are frequently used to describe heavy-ion collisions at intermediate energy. The BUU model [25] is based on one-body theory, which is described in the model by a calculation of the one-body phase-space density function. However, it is difficult to treat correlations and fragmentation in heavy-ion collisions with BUU. The QMD model [26] incorporates the important quantum features of BUU theory, explicitly treating the nucleon correlation information through the time evolution of the collision. It is able to describe the fluctuations that lead to the final fragmentation of the nuclear system. This is a major improvement over BUU. The QMD model is quite successful in describing collective effects such as bounce-off and squeeze-out. However, it fails in reproducing the fragment multiplicities observed experimentally. Nevertheless, the QMD and BUU models describe the initial non-equilibrium stage of the collision in reasonable detail and should predict the pre-thermalization nucleon emission and the formation of highly excited pre-fragments.

To investigate the persistence of a binary character, even for central collisions, and the formation of intermediate-velocity remnant in light heavy-ion collisions, we have performed

BUU calculations for ^{35}Cl+^{12}C at 43MeV/nucleon. The BUU equation has been solved with the parallel ensemble method [65]:

$$\frac{\partial f_1}{\partial t} + v \cdot \nabla_r f_1 - \nabla_r U \cdot \nabla_p f_1 =$$
$$\frac{4}{(2\pi)^3} \int d^3k_2 d\Omega \frac{d\sigma_{nn}}{d\Omega} v_{12} [f_3 f_4 (1-f_1)(1-f_2) - f_1 f_2 (1-f_3)(1-f_4)]. \quad (3)$$

In equation (2), $f = f(r,p,t)$ is the Wigner transformation of the one-body density matrix, $d\sigma_{nn}/d\Omega$ and v_{12} are the in-medium cross section and the relative velocity for the colliding nucleons respectively, and U is the total mean-field potential which consists of the Coulomb potential and the nuclear potential with isoscalar and symmetry terms. During our calculations, we used parameters for the equation of state (EOS) which correspond to values of nuclear compressibility at K=380 MeV (stiff EOS). For simplicity, $\sigma_{nn}(\theta,\phi)$ is chosen to be isotropic and energy-independent. The mean-field and the Pauli-blocking factors in the collision integral are averaged over an ensemble of 200 parallel simulations.

Figure 16 shows the time evolution of density profiles on the reaction plane for three impact parameters with a BUU model. For the calculation at b = 3.0 fm, a single deformed residue is still present at t = 220 fm/c. In contrast, the separated projectile-like and target-like fragments begin to show at slightly larger impact parameter b = 3.5 fm and become distinct at b = 4.0 fm. So, in this calculation, the critical impact parameter is 3.5 fm for the transition from the one body to the two body process. However, the calculation cannot produce neck fragments or an intermediate-velocity remnant in semi-peripheral collisions (between 2 and 4 fm). BUU simulations using a lower value of nuclear compressibility (soft EOS) were similar.

Recently, Sobotka [66] has performed BUU calculations for ^{136}Xe+^{208}Bi system at 28 MeV/nucleon considering a simple asymmetry-dependent term in the potentials which conspired to create reasonable neutron "skins" for heavy nuclei. Compared to calculations done with more commonly used equation of state, the calculations produced neutron-rich neck regions with higher probability. Neutron skin effects were shown to be a possible origin of neck-like structure in heavier systems. These effects cannot be considered in "neutron-

poor" systems such as $^{35}Cl+^{12}C$ studied here. A possible origin of neck-like structure for light heavy-ion systems is dynamical fluctuations. Colonna et. al [67] have implemented a fluctuating term into the BUU equation, arising from consideration of the random nature of the nucleon-nucleon collision integral. Their calculations predicted the existence of an intermediate neck region and the direct emission of intermediate mass fragments from the region.

To study the important role of mean field instabilities which originate from dynamical fluctuations in the reaction dynamics, we have performed QMD calculations for the $^{35}Cl+^{12}C$ system at 43 MeV/nucleon. Details about the code may be found in ref. [68]. Here we summarize briefly the relevant properties. In the model, each nucleon of two colliding nuclei is described by a Gaussian in momentum and coordinate space:

$$f_i(r,p,t) = \frac{1}{(\pi\hbar)^3} exp\{-\frac{[r-r_{i0}(t)]^2}{2L} - [p-p_{io}(t)]^2\frac{2L}{\hbar^2}\}, \tag{4}$$

where r_{i0} and p_{i0} are the centroids of the ith particle in coordinate and momentum space and $2L$ is the characteristic width of the wave packet. The nucleons interact via a potential during the collision. The interaction used here consists of a local Skyrme two- and three-particle interaction, a Coulomb and a Yukawa interaction. Neutrons and protons are distinguished in the interaction.

With these Gaussian nucleon distributions, the interactions lead to the following Hamiltonian:

$$H = \sum_i \frac{p_i^2}{2m} + V^{loc} + V^{Yuk} + V^{coul}. \tag{5}$$

The short-range interaction is taken into account in the same way as in the BUU models via a stochastic scattering term: two nucleons can scatter if the spatial distance of the centroids of their Gaussians is smaller than $\sqrt{\sigma_{tot}/\pi}$. The free nucleon-nucleon cross section is modified in the medium by the Uehling-Uhlenbeck blocking factors. The Pauli blocking probability of the final states is determined by the overlap of the two nucleons in phase space with all other nucleons. If a collision is blocked, the momenta of the scattering parameters

prior to the scattering are restored. We define the fragments at the end of the reaction using a common minimum spaning tree procedure. If the centroids of their wave packets have a spatial relationship $d_0 \leq 3fm$, two nucleons are considered to be bound in a fragment.

For the nuclear ground state, Fermi motion generated by the Pauli exclusion principle has been simulated by a momentum-dependent repulsive potential. The parametrized gaussian Pauli potential [69] is defined as:

$$E_{pau} = \frac{1}{2}\sum_{i\neq j} V^0_{pau}[\frac{\hbar}{q_0 p_0}]^2 exp[-\frac{r^2_{ij}}{2q^2_0} - \frac{p^2_{ij}}{2p^2_0}]\delta_{\tau_i\tau_j}\delta_{\sigma_i\sigma_j}, \tag{6}$$

where σ_i,τ_i denotes the spin and isospin index of nucleon i. With such a potential the total energy of the "free" Fermi gas is given by E^{FG}_{tot}=E_{kin}+E_{pau}. The parameters for the equation of state (EOS) and Pauli potential used in the calculation are taken from Ref [70], which correspond to a stiff EOS parameter of K=380 MeV.

The implementation of the Pauli potential into the dynamical QMD model yields two major improvements relative to earlier models [70]. Firstly, the ground states are well defined; this yields stable initial nuclei. This is very important for QMD model to be used in the Fermi energy region, $E_{lab} \approx 30$ MeV/nucleon [71,72]. Secondly, the excitation energy of the pre-fragments can be determined with respect to the true ground state and used to describe the long-term behavior of those fragments in an independent model such as a statistical decay model.

For a systematic study, we generated several thousand events, with the number of events contained in a given domain of impact parameter proportional to the cross section. For each time step, the momenta and the position of all nucleons were stored and the spatial distribution of the nucleons was investigated to examine the formation of the fragments.

After the collision has taken place, the system will continue to emit particles both in the pre-thermalization and the quasi-thermalization processes. Therefore the masses and excitation energies of pre-fragments are sensitive to the freeze-out time at which observables are evaluated. During the calculation, we switched off the QMD calculations at a time of 120 fm/c after the first contact of two colliding nuclei (at t=0 the projectile and target surfaces

are separated by approximately 2.0 fm). At this time the fast pre-thermalization processes are terminated (the time for pre-thermalization emission is nearly 70 fm/c) and the mass and excitation energies of the pre-fragments do not change rapidly with time, which can be seen as evidence that the nuclear system is approaching thermal equilibrium before breakup.

Figure 17 shows the impact parameter b versus mass distribution of pre-fragments for ^{35}Cl+^{12}C at 43 MeV/nucleon reaction with QMD calculations at t=120 fm/c. In the case of a head-on collision, we see clearly that the fragment mass distribution is composed of a heavy fragment $A_f \approx 41$ and a few nucleons. This means that the reaction mechanism is complete or incomplete fusion (one-source events). With a slight increase of impact parameter, in addition to the incomplete fusion process, we can observe two-fragment events in the mid-central region. From the time evolution of the spatial distribution of nucleons, we observe such events originating from incompletely fused system reseparated into two fragments, from which nucleons and/or clusters continue to escape (two-source events). The process is similar to asymmetric fission at lower energy heavy-ion reaction. In the semi-peripheral region $b \approx$ 3.5 fm, in addition to one- and two-fragment events, we also observe three-fragment events (three-source events). For peripheral region, b$\geq$ 6.0 fm, we see clearly that the fragment mass distribution is composed of two heavy fragments $A_f \approx 34$ and $A_f \approx 10$ respectively, which could be attributed to target-like fragment (TLF) and projectile-like fragment (PLF). Here, the collision process is just a dissipative binary process as in deep-inelastic collisions.

In fig. 18, we show the differential cross section $d\sigma/db$ for one, two and three IMF as a function of impact parameter b for ^{35}Cl+^{12}C reaction at 43 MeV/nucleon as predicted from our QMD calculations. The IMF are defined here as fragments with $Z \geq 3$. The cross section of one-IMF events, which approximately correspond to the incomplete fusion at small impact parameter, is 15% of the reaction cross section. It is still larger than the 4% from experimental results [15]. Dissipative binary collisions (two-IMF events) are the dominant reaction process; they account for about 80% of the cross section and occur almost at all impact parameters, even in central collisions. The cross section for three-IMF events is only of the order of 3% of the cross section. At b=3.5 fm, the cross section of one-IMF events is

equal to that of two-IMF events. This prediction is consistent with the BUU calculations.

To search for the formation of an intermediate-velocity remnant, we produced a contour plot of the IMF velocity components (v_z) versus position z on beam direction for three IMF events, as shown in fig. 19. An interesting result is that the IMF can be classified into three groups. A first group is in the region of $z \geq$12 fm and $v_z \geq$3 cm/ns, representing fragment with a mass $A_f \approx 31$, and it could be attributed to the PLF. A second group is in the region of $z \leq$2.0 fm and $v_z \leq$0 cm/ns, $A_f \approx 7$, and could be attributed to the TLF. For the remaining group, its velocity is near to 0.5 fm/c and $z \approx 6$, $A_f \approx 7$. Because its character is similar to what is called the participant-spectator process in higher energy heavy-ion collision, we consider it as an intermediate-velocity remnant. It is concentrated in mid-peripheral collisions as shown in fig. 18. In summary, the BUU model fails to yield any indication of an intermediate source, while QMD appears to predict a small such component

B. Alpha Cluster Molecular Dynamics

The idea that the nuclear structure of a small nucleus with even Z and $A = 2Z$ can be approximated by clusters of α particles has been proposed since the 1950's [73]. Recently however there has been a renewed interest for this particular field in experiments below 10 MeV/nucleon (see Ref. [74] for a recent review). The study of nuclear clusters is ideal for the intermediate energy range since an alpha structure driven collision is halfway between the mean field effects of low energy reaction (<10 Mev/nucleon) and the quasi-exclusive nucleon-nucleon interactions present at high energy (>100 MeV/nucleon). Both mechanisms are known to be important in this energy range [75–77].

A dynamical alpha-cluster model for projectile break-up has been developed by Möhring et al. [7,27]. It is based on two complementary assumptions: An α-α potential deduced from ATDHF calculations [78] and an additional energy conserving random walk interaction used to reproduce large angle scattering. Originally the model was used exclusively for projectile break-up of light nuclei on heavier targets, modelled via surface friction, leading either to

fragmentation of the alpha clusters or to incomplete fusion of the projectile and the target [7]. In the analysis of the $^{32}S+^{197}Au$ system at 26 MeV/nucleon [5], comparison with the alpha-cluster model leads to the conclusion that the branching ratios for channels with two IMF coming from the projectile break-up are dominantly fed by a non-sequential production mode.

The model was also used for a light symmetric system, $^{12}C+^{12}C$, where both nuclei are treated in the the alpha-cluster model [79]. In this study the energy spectra of alpha particles cannot be reproduced by alpha-cluster dynamics alone and a contribution from a compound nucleus had to be added to fit the experimental data. However, the forward-angle cross-sections of alpha-particle energy were correctly reproduced without any free parameters. Since the simplifications present in the model, such as neglecting nucleonic degrees of freedom, could be the cause of some of the discrepancies between data and simulations, improved versions of the model may offer a better picture of reaction dynamics in the intermediate energy range. No intermediate source formation was apparent in either the projectile break-up or central collision using Möhring's alpha-cluster molecular dynamics model.

Recently a new model of alpha-cluster molecular dynamics was developed by López and Robinson [80]. Using the alpha-alpha potential of Möhring et al. simulations of reactions of $^{32}S + ^{12}C$ and $^{32}S + ^{24}Mg$ were studied at energies of 5.4, 8.4, and 14.2 MeV/A. The selection of projectile and targets was made to reproduce as closely as possible the reactions studied experimentally in this work. The energies were selected to show where the transition from a single-velocity source to two sources takes place. In contrast to the Möhring calculation, López and Robinson did not use the random interaction responsible for large-angle scattering nor did they use interparticle friction.

The unfiltered velocity distributions obtained for the particles resulting from these simulations for alphas, beryllium (di-alphas), etc. show contributions of a single-velocity source (for lower energies) and of a projectile-like source and a second, slower, target-like source, at higher energies. These results indeed fail to indicate the existence of a third, intermediate-velocity, source. Presumably the lack of alpha-alpha friction and angular momentum in the

calculations are responsible for this behavior.

C. Di-nuclear orbiting

In the di-nuclear orbiting model [28–34] two colliding nuclei are trapped by the attractive nuclear interaction and lose energy via friction while rotating one around the other. As the deflection angle, given by grazing angle minus scattering angle (qualitatively similar to the flow angle used in the experimental analysis) increases, the final kinetic energy of the system decreases. This orbiting process is limited by two extreme values of angular momentum, l_{max} where the scattering angle is very close to the grazing angle, and l_{crit} where the Coulomb and centrifugal forces are balanced, and which usually leads to a fused system in the 5-10 MeV/nucleon energy range [28].

The surface friction model developed by Gross and Kalinowski [29,81] is a combination of the optical model nucleon-nucleus potential and of the assumption that the two ions move on a classical orbit under the presence of a friction force. The friction is modelled by an anisotropic position-dependent tensor with a radial-radial component much larger than the tangential-tangential component. The main achievement of the model is to give an appropriate description of how the two ions undergo a very inelastic collision when the reaction is peripheral, and fuse when it is more central. The model's predictions of l_{crit} (fusion) are in good agreement with low energy experimental data. The same frictionnal forces are used in the molecular dynamics calculations of Möhring et al. discussed in the last section.

Di-nuclear orbiting was found to be an even more important contribution to the reaction mechanism in lighter sytems. Shapira et al. [31] showed that while energy spectra in the ^{28}Si + ^{12}C reaction at around 4 MeV/nucleon indicate strong if not complete damping, there is a large component in the angular distribution around $\Theta_{c.m.}$=180°, a feature typical of a fully developed orbiting process. In other heavy-ion collisions experiment at low energy (below 10 Mev/nucleon), comparison of data to orbiting calculations and to compound nucleus

formation clearly favors orbiting [33]. Such orbiting data of relatively light heavy ions (such as $^{28}Si + ^{12}C$ and $^{24}Mg + ^{12}C$) were interpreted as demonstrating a strong entrance channel dependence at low energy [34]. However, no entrance channel effects were observed for other slightly different heavy ion combinations (such as $^{35}Cl + ^{12}C$ compared to $^{31}P + ^{16}O$) and the disappearance of the orbiting yield may be explained by the presence of quasi-molecular resonance states [82–84] where orbiting occurs only for well-matched energetic and angular momentum states [31]. The origin of the orbiting mechanism is still an open question, though possibly related to the exchange of nucleons.

In a recent experiment in the Fermi energy range (30 MeV/nucleon) involving relatively heavy ions ($^{136}Xe + ^{209}Bi$), Baldwin et al. [8] concluded that the reaction dynamics are similar to what is expected from di-nuclear dissipative orbiting based on the strong correlations between the deflection angle of massive fragments and various dissipation observables. The analysis also shows possible experimental evidence for a "nuclear rainbow" [32] in the data, where the balance between Coulomb and nuclear forces produces a local minimum. The overall reaction mechanism could not be reproduced quantitatively by either a nucleon-exchange model or dynamical Boltzmann-Uehling-Uhlenbeck (BUU) simulations.

In regards to the formation of an intermediate-velocity remnant, the orbiting mechanism in rather peripheral heavy-ion collisions could be linked to the appearance of a neck-like structure [16–18,32] between the two nuclei. It has been proposed that this neck structure is caused by a neutron-skin effect and isopin dependance [66,85]. There are some discrepancies between low-energy reactions, where central collisions involve the complete fusion of the system, and reactions in the Fermi energy range, where the system appears to remain di-nuclear even though a a huge amount of dissipation is involved [10,12,15]. However, the orbiting model offers a simple macroscopic picture that covers the whole range of impact parameters for energies of a few to a few tens of MeV/nucleon. Nevertheless, as discussed in section IV.A, there is as yet no experimental evidence of di-nuclear orbiting for reactions of light ions in the intermediate enery range and the formation of a neck is dubious in these systems because of the generally "neutron-poor" character of the ions (^{35}Cl, ^{24}Mg or ^{12}C for

example) when compared to heavier systems such as $^{208}Pb+^{197}Au$ or $^{136}Xe+^{209}Bi$.

D. Nuclear Tranparency in the Fermi energy range

The problem of nuclear transparency in the Fermi energy range was addressed in 1980 by Collins and Griffin [86]. In this calculation the mean free path (λ) of the nucleon in a nuclear Fermi gas at finite temperature is obtained using free nucleon-nucleon cross section with suppression according to the Pauli exclusion principle, thus increasing λ. If this mean free path can be considered "large" when compared to the nuclear radius, it has an important effect on the organization of the nuclear structure in very excited states. Furthermore the ensuing appearance of free nucleons with trajectories unhindered by the mean-field effect of the nucleus bears a direct relation to the notion of preequilibrium emission of protons and neutrons, commonly encountered in heavy ion reaction analyses [39,43].

Based on their calculations, the authors of ref. [86] conclude that for a temperature of about 4.5 MeV, λ is of the order of 10 fm, about the diameter of a A$\approx$125 nucleus. Below that temperature the nucleus can then be considered a "small" object. These results underestimate the λ calculated from the phenomenological optical-model. Since the temperature attained in intermediate energy heavy ion collisions is of the order of 5 MeV [7,75,87–90], we can assume that nuclear transparency is a factor to be considered.

However, from a macroscopic (or collective) point of view, the effects of nuclear transparency in collisions between two nuclei with constant density would not lead to the formation of an intermediate-velocity remnant in a dissipative binary scenario but would be closer to the preequilibrium projectile-like and target-like emission in an incomplete fusion reaction, a mechanism which has been shown to be at least partly incompatible with heavy ion reactions dynamics in the Fermi energy range [9–12,14].

E. Expansion and hollow configurations

As we have seen in the previous sections, neither dynamical simulations nor more classical macroscopic mechanisms offer a complete explanation of dissipative binary collisions involving rather light ions and intermediate-velocity remnant formation in the Fermi energy range. There is one common feature for all the theoretical predictions: they use, implicitly or explicity, a standard nuclear density. This nuclear density is basically constant from the center to the external radius of a spherical nucleus. It would also decrease uniformly through isotropic expansion, because of heating or compression, after a heavy ion collision (see, for example, Bertsch and Siemens [91]),

Introducing new expressions for density and temperature as a function of radius and time with a generalization of the analytical hydrodynamical model of an expanding "fireball" from previous work by Bondorf et al. [92], Borunda and López [35] have investigated the formation of hollow configurations following the expansion phase in heavy-ion collisions. The hydrodynamical behavior of the hot and dense nucleus shows a rapid expansion of the nuclear system. Remarkably this expansion is non-uniform spatially, producing a region of subnormal density. The calculations also predict the appearance of a high-density region. These intriguing configurations cannot yet be followed to the final freeze-out density and actual fragmentation of the nucleus. However, they could offer new insight into dynamical multifragmentation.

The appearance of such hollow configurations in the possibly expanding overlapping region of a di-nuclear system would provide a phenomenological explanation of the macroscopic reaction dynamics in intermediate-energy heavy ion collisions. It could account for both the persistence of the dissipative binary mechanism (possibly separated by a low density region) and the formation of an intermediate-velocity remnant (high density region) producing most of the IMF. It would also account for the observed low transverse velocity of IMF in the intermediate zone, as they are not emitted from a thermal source but are rather remnants of a dynamical reaction. The evolution of a "hot-zone" in nuclear matter following heavy

ion collisions was examined by Jakobsson, Karlsson and López [93]. Although it features pre-thermalization emission of light particles, it does not predict the formation of IMF in the participant zone.

We thus see that due to numerical and other approximations, most models used in this energy regime fail to predict the existence of a third source of IMF, with the notable exception of the QMD approach, although the physical implications are hard to pinpoint in that case. We think that the formation of hollow configurations, and possibly other expansion mechanisms, should be investigated further in regards to the formation of intermediate-velocity remnant and IMF production in general.

V. CONCLUSION

We have investigated the formation of an intermediate-velocity remnant and neck-like structure in intermediate energy reactions involving "light" heavy ions. For the two nearly-symmetric systems (^{35}Cl+^{12}C and ^{35}Cl+^{24}Mg), the presence of an intermediate-velocity remnant, seen in the velocity maps of intermediate mass fragments, is evaluated to be a maximum of 20% of the all analysed events in central/mid-central reactions. The actual cross section for the process is lower and is roughly estimated at 10%. For bigger nuclear systems (^{35}Cl+^{197}Au), the appearance of a intermediate-velocity remnant and/or neck-like structure has also been observed. For bigger nuclear systems, more than one IMF remnant can be expected.

We have performed BUU and QMD calculations for the reaction ^{35}Cl+^{12}C at 43 MeV/nucleon. With our choice of input parameters, BUU calculations give a critical impact parameter of 3.5 fm for the transition from a one-body to a two-body process. The model cannot produce intermediate-velocity remnants in semi-peripheral collisions as is observed in the experimental results. QMD calculations which preserve dynamical fluctuations through the time evolution of the collision can produce intermediate-velocity remnants at $b \approx 4$ fm for the ^{35}Cl+^{12}C reaction. With the QMD model, the most probable origin of a neck-like structure for light heavy-ion system lies in dynamical fluctuations. The calculated cross section for intermediate-velocity remnant events is less than 3% of cross section at 43 MeV/nucleon. For the systems studied, the calculations predict that binary dissipative collisions are a dominant reaction process, occuring over a large range of impact parameters, and even in central collisions.

Investigations with other theoretical and phenomenological models, such as orbiting, nuclear transparency and molecular dynamics, failed to reproduce the trends found in the data. The possible expansion of an overlapping "hot zone" of contact between the nuclei, and the formation of hollow configurations, were assessed as possible explanations for the remnant formation.

Another possible explanation for the presence of an intermediate-velocity remnant would be deformation, occuring during the collision, of the heaviest partner in asymmetric systems, or both projectile and the target in symmetric systems. This deformation is not predicted by actual dynamical models. Results from more complete experiments, possibly including complete isotopic resolution, and more detailed dynamical simulations are needed before the mechanisms can be definitively identified. However, from our results, it is evident that along with statistical mechanisms, reaction dynamics play a major role in the production mechanism of IMF.

ACKNOWLEDGMENTS

We would like to thank D. Durand and J.-P. Wieleczko for the use of their statistical codes, G. Peilert for the QMD code and J.B. Natowitz for the BUU code. This work was supported in part by the Natural Sciences and Engineering Research Council of Canada.

REFERENCES

[1] D. Jouan, B. Borderie, M.F. Rivet, C. Cabot, H. Fuchs, H. Gauvin, C. Grégoire, F. Hanappe, D. Gardes, M. Montoya, B. Remaud, and F. Sebille, Z. Phys. A **340**, 63 (1991).

[2] M. Colonna, N. Colonna, A. Bonasera, and M. DiToro, Nucl. Phys. **A541**, 295 (1992).

[3] J. Suro, Y.D. Chan, J.A. Scarpaci, R.G. Stokstad, K. Möhring, and T.C. Schmidt, Nucl. Phys. **A548**, 353 (1992).

[4] R. Wada, M. Gonin, M. Gui, K. Hagel, Y. Lou, D. Utley, B. Xiao, D. Miller, J.B. Natowitz, D. Fabris, G. Nebbia, R. Zanon, B. Chambon, B. Cheynis, A. Demeyer, D. Drain, D. Guinet, X.C. Hu, C. Pastor, K. Zaid, J. Alarja, R. Bertholet, A. Giorni, A. Lleres, C. Morand, P. Stassi, L. Schussler, B. Viano, and P. Gonthier, Nucl. Phys. **A548**, 471 (1992).

[5] C. Schwartz, H. Fuchs, H. Homeyer, K. Möhring, T. Schmidt, A. Siwek, A. Sourell, W. Terlau, and A. Budzanowski, Z. Phys. A **345**, 29 (1993).

[6] G. Peilert, H. Stöcker, and W. Greiner, Rep. Prog. Phys. 57, 533 (1994).

[7] H. Fuchs and K. Möhring, Rep. Prog. Phys. 57, 231 (1994).

[8] S.P. Baldwin, B. Lott, B.M. Szabo, B.M. Quednau, W.U. Schröder, J. Töke, L.G. Sobotka, J. Baretto, R.J. Charity, L. Gallamore, D.G. Sarantites, D.W. Stracener, and R.T. de Souza, Phys. Rev. Lett. **74** , 1299 (1995).

[9] Y. Larochelle, L. Beaulieu, G. Anctil, B. Djerroud, D. Doré, R. Laforest, J. Pouliot, R. Roy, M. Samri, C. St-Pierre, G.C. Ball, D.R. Bowman, A. Galindo-Uribarri, E. Hagberg, D. Horn, D. Guinet, and P. Lautesse, Phys. Rev. C **53**, 823 (1996).

[10] B. Lott, S.P. Baldwin, B.M. Szabo, B.M. Quednau, W.U. Schröder, J. Tóke, L.G. Sobotka, J. Barreto, R.J. Charity, L. Gallamore, D.G. Sarentites, and D.W. Stracener,

Phys. Rev. Lett. **68**, 3141 (1992).

[11] B.M. Quednau, S.P. Baldwin, B. Lott, W.U. Schröder, B.M. Szabo, J. Tóke, D. Hilscher, U. Jahnke, H. Rossner, S. Bresson, J. Galin, D. Guerreau, M. Morjean, and D. Jacquet, Phys. Lett. **B309**, 10 (1993).

[12] J.F. Lecolley, L. Stuggé, M. Aboufirassi, A. Badala, B. Bilwes, R. Bougault, R. Brou, F. Cosmo, J. Colin, D. Durand, J. Galin, A. Genoux-Lubain, D. Guerreau, D. Horn, D. Jacquet, J.L. Laville, F. Lefebvres, C. LeBrun, J. Lemière, O. Lopez, M. Louvel, M. Mahi, M. Morjean, C. Paulot, A. Péghaire, N. Prot, G. Rudolf, F. Scheibling, J.C. Steckmeyer, B. Tamain, and S. Tomasevic, Phys. Lett. **B 325**, 317 (1994).

[13] Y. Larochelle, G.C. Ball, L. Beaulieu, B. Djerroud, D. Doré, A. Galindo-Uribarri, P. Gendron, E. Hagberg, D. Horn, E. Jalbert, R. Laforest, J. Pouliot, R. Roy, M. Samri, and C. St-Pierre, Phys. Lett. **B 352**, 8 (1995).

[14] J. Péter, S.C. Jeong, J.C. Angélique, G. Auger, G. Bizard, R. Brou, A. Buta, C. Cabot, Y. Cassagnou, E. Crema, D. Cussol, D. Durand, Y. El Masri, P. Eudes, Z.Y. He, A. Kerambrun, C. Lebrun, R. Legrain, J.P. Patry, A. Péghaire, R. Régimbart, E. Rosato, F. Saint-Laurent, J.C. Steckmeyer, B. Tamain, and E. Vient, Nucl. Phys. **A593**, 95 (1995).

[15] L. Beaulieu, Y. Larochelle, L. Gingras, G.C. Ball, D.R. Bowman, B. Djerroud, D. Doré, A. Galindo-Uribarri, D. Guinet, E. Hagberg, D. Horn, R. Laforest, P. Lautesse, R. Roy, M. Samri, and C. St-Pierre, Phys. Rev. Lett. **77** , 462 (1996).

[16] C.P. Montoya, W.G. Lynch, D.R. Bowman, G.F. Peaslee, N. Carlin, R.T. de Souza, C.K. Gelbke, W.G. Gong, Y.D. Kim, M.A. Lisa, L. Phair, M.B. Tsang, J.B. Webster, C. Williams, N. Colonna, K. Hanold, M.A. McMahan, G.J. Wozniak, and L.G. Moretto, Phys. Rev. Lett. **73**, 3070 (1994).

[17] J. Tõke, B. Lott, S.P. Baldwin, B.M. Quedneau, W.U. Schröder, L.G. Sobotka, J.

Barreto, R.J. Charity, D.G. Sarantites, D.W. Stracener, and R.T. de Souza, Phys. Rev. Lett. **75**, 2920 (1995).

[18] J.F. Lecolley, L. Stuggé, M. Aboufirassi, B. Bilwes, R. Bougault, R. Brou, F. Cosmo, J. Colin, D. Durand, J. Galin, A. Genoux-Lubain, D. Guerreau, D. Horn, D. Jacquet, J.L. Laville, F. Lefebvres, C. Le Brun, O. Lopez, M. Louvel, M. Mahi, C. Meslin, M. Morjean, A. Péghaire, G. Rudolf, F. Scheibling, J.C. Steckmeyer, B. Tamain, and S. Tomasevic, Phys. Lett. **B 354**, 202 (1995).

[19] G.D. Westfall, J. Gosset, P.J. Johansen, A.M. Poskanzer, W.G. Meyer, H.H. Gutbrod, A. Sandoval, and R. Stock, Phys. Rev. Lett. **37**, 1202 (1976).

[20] R. Stock, Phys. Rep. **135**, 259 (1986).

[21] B. Borderie, M.F. Rivet, and L. Tassan-Got, Ann. Phys. Fr. **15**, 287 (1990).

[22] C.A. Pruneau, G.C. Ball, E. Hagberg, D. Horn, S. Gilbert, L. Potvin, C. Rioux, C. St-Pierre, T.E. Drake, A. Galindo-Uribarri, G. Zwartz, D.A. Cebra, S. Howden, J. Karn, C.A. Ogilvie, A. Vander Molen, G.D. Westfall, W.K. Wilson, and J.S. Winfield, Nucl. Phys. **A534**, 204 (1991).

[23] J.P. Alard, Z. Basrak, N. Bastid, I.M. Belayev, M. Bini, Th. Blaich, R. Bock, A. Buta, R. Čaplar, C. Cerruti, N. Cindro, J.P. Coffin, M. Crouau, P. Dupieux, J. Erö, Z.G. Fan, P. Fintz, Z. Fodor, R. Freifelder, L. Fraysse, S. Frolov, A. Gobbi, Y. Grigorian, G. Guillaume, N. Herrmann, K.D. Hildenbrand, S. Hölbling, O. Houari, S.C. Jeong, M. Jorio, F. Jundt, J. Kecskemeti, P. Koncz, Y. Korchagin, R. Kotte, M. Krämer, C. Kuhn, I. Legrand, A. Lebedev, C. Maguire, V. Manko, T. Matulewicz, G. Mgebrishvili, J. Mösner, D. Moisa, G. Montarou, P. Morel, W. Neubert, A. Olmi, G. Pasquali, D. Pelte, M. Petrovici, G. Poggi, F. Rami, W. Reisdorf, A. Sadchikov, D. Schüll, Z. Seres, B. Sikora, V. Simion, S. Smolyankin, U. Sodan, N. Taccetti, K. Teh, R. Tezkratt, M. Trzaska, M.A. Vasiliev, P. Wagner, J.P. Wessels, T. Wienold, Z. Wilhelmi, D. Wohlfarth,

and A.V. Zhilin, Phys. Rev. Lett. **69**, 889 (1992).

[24] L. Stuttgé, J.C. Adloff, B. Bilwes, R. Bilwes, F. Cosmo, M. Glaser, G. Rudolf, F. Scheibling, R. Bougault, J. Colin, F. Delaunay, A. Genoux-Lubain, D. Horn, C. le Brun, J.F. Lecolley, M. Louvel, J.C. Steckmeyer, J.L. Ferrero, Nucl. Phys. **A539**, 511 (1992).

[25] G. F. Bertsch and S. Das Gupta, Phys. Rep. **160**, 190 (1988).

[26] J. Aichelin and H. Stöcker, Phys. Lett. **B 176**,14 (1986).

[27] K. Möhring, T. Srokowski, D.H.E. Gross, and H. Homeyer, Phys. Lett. **B 203**, 210 (1988).

[28] J. Wilczyński, Phys. Lett. **B 47**, 484 (1973).

[29] D.H.E. Gross and H. Kalinowski, Phys. Lett. **B 48**, 302 (1974).

[30] J.P. Bondorf, M.I. Sobel, and D. Sperber, Phys. Rep. **15**, 83 (1974).

[31] D. Shapira, R. Novotny, Y.D. Chan, K.A. Erb, J.L.C. Ford Jr., J.C. Peng, and J.D. Moses, Phys. Lett. **B 114**, 111 (1982).

[32] W.U. Schröder and J.R. Huizenga, in Treatise on Heavy-Ion Science, edited by D.A. Bromley (Plenum, New York and London 1984), Vol. 2, p. 115.

[33] B. Shiva Kumar, D. Shapira, P.H. Stelson, S. Ayik, B.A. Harmon, K. Teh, and D.A. Bromley, Phys. Rev. C **37**, 652 (1988).

[34] B. Shiva Kumar, D.J. Blumenthal, S.V. Greene, J.T. Mitchell, D.A. Bromley, D. Shapira, J. Gomez del Campo, A. Ray, and M.M. Hindi, Phys. Rev. C **46**, 1946 (1992).

[35] M. Borunda and J.A. López, Il Nuov. Cim. **107**, 2773 (1994).

[36] L. Beaulieu, Ph. D. Thesis, Université Laval, 1996 (unpublished).

[37] C. Pruneau, D. Horn, M.G. Steer, R.B. Walker, T. Whan, C. Rioux, R. Roy, C. St-Pierre, T.E. Drake, and A. Galindo-Uribarri, Nucl. Inst. and Meth. **A297**, 404 (1990).

[38] Y. Larochelle, L. Beaulieu, B. Djerroud, D. Doré, P. Gendron, E. Jalbert, R. Laforest, J. Pouliot, R. Roy, M. Samri, and C. St-Pierre, Nucl. Instr. and Meth. in Phys. Res. **A348**, 167 (1994).

[39] H. Morgenstern, W. Bohne, W. Galster, K. Grabisch, and A. Kyanowski, Phys. Rev. Lett. **52**, 1104 (1984).

[40] N. Colonna, R.J. Charity, D.R. Bowman, M.A. McMahan, G.J. Wozniak, L.G. Moretto, G. Guarino, A. Pantaleo, L. Fiore, A. Gobbi, and K.D. Hildenbrand, Phys. Rev. Lett. **62**, 1833 (1989).

[41] K. Hagel, A. Péghaire, G.M. Jin, D. Cussol, H. Doubre, J. Péter, F. Saint-Laurent, G. Bizard, R. Brou, M. Louvel, J.P. Patry, R. Regimbart, J.C. Steckmeyer, B. Tamain, Y. Cassagnou, R. Legrain, C. Lebrun, E. Rosato, R.L. McGrath, S.C. Jeong, S.M. Lee, Y. Nagashima, T. Nakagawa, M. Ogihara, J. Kasagi, and T. Motobayashi, Phys. Lett. **B 229**, 20 (1989).

[42] Y. Blumenfeld, N. Colonna, P. Roussel-Chomaz, D.N. Delis, K. Hanold, J.C. Meng, G.F. Peaslee, Q.C. Sui, G.J. Wozniak, L.G. Moretto, B. Libby, A.C. Mignerey, G. Guarino, N. Santoruvo, and I. Iori, Phys. Rev. Lett. **66**, 576 (1991).

[43] A. Malki, J.P. Coffin, G. Guillaume, F. Jundt, K. Krishan, F. Rami, P. Wagner, P. Fintz, M. Zahar, M. Gonin, B. Heusch, M. Ohta, B. Rastegar, D. Rebreyend, F. Merchez, J. Mistretta, and S. Kox, Z. Phys. A **339**, 283 (1991).

[44] G. Nebbia, J.A. Ruiz, D. Fabris, G. Viesti, R.H. Burch, F. Gramegna, G. Prete, A. Giorni, A. Lleres, J.B. Viano, B. Chambon, B. Cheynis, A. Demeyer, D. Drain, D. Guinet, X.C. Hu, M. Gonin, K. Hagel, J.B. Natowitz, R. Wada, and P.L. Gonthier, Phys. Rev. C **45**, 317 (1992).

[45] K. Hanold, L.G. Moretto, G.F. Peaslee, G.J. Wozniak, D.R. Bowman, M.F. Mohar, and D.J. Morissey, Phys. Rev. C **48**, 723 (1993).

[46] S. Datta, K. Krishan, and S. Bhattacharya, Z. Phys. A **353**, 49 (1995).

[47] J.A. Scarpaci, Y. Chan, D. DiGregorio, B.A. Harmon, J. Pouliot, R.G. Stokstad, and J. Suro, Phys. Rev. C **52**, 764 (1995).

[48] D. Durand, Nucl. Phys. **A541**, 266 (1992).

[49] J. Cugnon and D. L'Hote, Nucl. Phys. **A397**, 519 (1983).

[50] H. Ströbele, R. Brockmann, J.W. Harris, F. Riess, A. Sandoval, R. Stock, K.L. Wolf, H.G. Pugh, L.S. Schroeder, R.E. Renfordt, K. Tittel, and M. Maier, Phys. Rev. C **27**, 1349 (1983).

[51] N. Cindro, M. Korolija, E. Bětàk, and J.J. Griffin, Phys. Rev. Lett. **66**, 868 (1991).

[52] A. Hakim, A. Fahli, M. Ohta, G. Guillaume, J.P. Coffin, P. Fintz, J. Jundt, A. Malki, F. Rami, B. Rastegar, P. Wagner, and M. Zahar, Il Nuov. Cim. **107**, 1587 (1994).

[53] W. Bauer and A. Botvina, Phys. Rev. C **52**, R1760 (1995).

[54] C. Brusati, M. Cavinato, E. Fabrici, E. Gadioli, and E. Gadioli-Erba, Z. Phys. A **353**, 57 (1995).

[55] T.C. Awes, S. Saini, G. Poggi, C.K. Gelbke, D. Cha, R. Legrain, and G.D. Westfall, Phys. Rev. C **25**, 2361 (1982).

[56] Z. Saddiki, Master Thesis, Université Laval, 1996 (unpublished).

[57] M. Blann and B. Remington, Phys. Rev. C **37**, 2231 (1988).

[58] J.P. Wieleczko, E. Plagnol, and P. Ecomard, Proceedings of the 2^{nd} TAPS Workshop 1994, ed. by Diaz, Martinez and Schutz, Guardemar , World Scientific 1995, p.145 .

[59] R. Laforest, Ph. D. Thesis, Université Laval, 1994 (unpublished).

[60] D. Doré, Ph. D. Thesis, Université Laval, 1994 (unpublished).

[61] A. Lleres, A. Giorni, H. Elhage, M.E. Brandan, A. J. Cole, P. Désesquelles, D. Heuer, A. Menchaca-Rocha, J. B. Viano, F. Benrachi, B. Chambon, B. Cheynis, D. Drain, and C. Pastor, Phys. Rev. C **48**, 2753 (1993).

[62] C.H. Dasso and G. Pollarolo, Comp. Phys. Comm. **50**, 341 (1988).

[63] R.J. Charity, M.A. McMahan, G.J. Wozniak, R.J. McDonald, L.G. Moretto, D.G. Sarantites, L.G. Sobotka, G. Guerino, A. Pantaleo, L. Fiore, A. Gobbi, and K.D. Hildenbrand, Nucl. Phys. **A483**, 371 (1988).

[64] J.A. López and J. Randrup, Comp. Phys. Comm. **70**, 92 (1990).

[65] W. Bauer, G. F. Bertsch, W.Cassing, and U. Mosel, Phys. Rev. **C 34**, 2127 (1986).

[66] L. Sobotka, Phys. Rev. C **50**, R1772 (1994).

[67] M. Colonna, M. Di Toro, and A. Guarnera, Nucl. Phys. A **589**, 160 (1995).

[68] J. Aichelin, Phys. Rep. **202**, 233 (1991).

[69] C. Dorso and J. Randrup, Phys Lett. B **215**, 611 (1988).

[70] G. Peilert, J. Konopka, H. Stöcker, W. Greiner, M. Blann, and M. G. Mustafa, Phys. Rev. C **46**, 1404 (1992).

[71] Toshiki Maruyama, Akira Ohnishi, and Hisashi Horiuchi, Phys. Rev C **42**, 386 (1990).

[72] Toshiki Maruyama, Akira Ohnishi, and Hisashi Horiuchi, Phys. Rev C **45**, 2355 (1992).

[73] H. Morinaga, Phys. Rev. **101**, 254 (1956).

[74] A.H. Wuosmaa, R.R. Betts, M. Freer, and B.R. Fulton, Ann. Rev. Nucl. Part. Sci. **45**, 89 (1995).

[75] D.H.E. Gross, Rep. Prog. Phys. **53**, 605 (1990).

[76] B. Tamain, Nuclear Collision from the Mean-Field into the Fragmentation Regime, Enrico Fermi School, Course CXII, Italy 1989, Elsevier Science Publishers B.V., North-Holland, (1991).

[77] L.G. Moretto and G. Wozniak, Ann. Rev. Nucl. Part. Sci. **43**, 379 (1993).

[78] D. Provoost, F. Grümmer, K. Goeke, and P.-G. Reinhard, Nucl. Phys. **A431**, 139 (1984).

[79] A. Szczurek, A. Budzanowski, L. Jarczyk, A. Magiera, K. Möhring, R. Siudak, and T. Srokowski, Z. Phys. A **338**, 187 (1991).

[80] T. Robinson , Master Thesis, University of Texas at El Paso, 1996 (unpublished).

[81] D.H.E. Gross and H. Kalinowski, Phys. Rep. **45**, 175 (1978).

[82] A. Ray, D. Shapira, J. Gomez del Campo, H.J. Kim, C. Beck, B. Djerroud, B. Heusch, D. Blumenthal, and B. Shiva Kumar, Phys. Rev. C **44**, 514 (1991).

[83] C. Beck, B. Djerroud, F. Haas, R.M. Freeman, A. Hachem, B. Heusch, A. Morsad, M. Vuillet-A-Cilles, and S.J. Sanders, Phys. Rev. C **47**, 2093 (1993).

[84] M. Papa, G. Cardella, A. Di Pietro, S.L. Li, A. Musumarra, G. Pappalardo, F. Rizzo, A. De Rosa, G. Inglima, M. La Commara, D. Pierroutsakou, and M. Romoli, Z. Phys. A **353**, 205 (1995).

[85] B. Jouault, V. de la Mota, F. Sébille, G. Royer, and J.F. Lecolley, Nucl. Phys. **A597**, 136 (1996).

[86] M.T. Collins and J.J. Griffin Nucl. Phys. **A348**, 63 (1980).

[87] J. Bondorf, R. Donangelo, I.N. Mishustin, and H. Schulz, Nucl. Phys. **A444**, 460 (1985).

[88] J. Pochodzalla, C.K. Gelbke, C.B. Chitwood, D.J. Fields, W.G. Lynch, M.B. Tsang,

and W.A. Friedman, Phys. Lett. **B 175**, 275 (1986).

[89] C.K. Gelbke and D.H. Boal, Progr. Part. Nucl. Phys. **19**, 33 (1987).

[90] D. Fox, D.A. Cebra, J. Karn, C. Parks, A. Pradhan, A. Vander Molen, J. van der Plicht, G.D. Westfall, W.K. Wilson, and R.S. Tickle, Phys. Rev. C **38**, 146 (1988).

[91] G. Bertsch and Philip J. Siemens, Phys. Lett. **B 126**, 9 (1983).

[92] J.P. Bondorf, S.I.A. Garpman, and J. Zimànyí, Nucl. Phys. **A296**, 320 (1978).

[93] B. Jakobsson, L. Karlsson, and J.A. López, Nucl. Phys. **A531**, 143 (1991).

FIGURES

FIG. 1. The CRL-Laval Array. See text for description.

FIG. 2. Reconstructed c.m. velocity from detected ions for events with $\Sigma Z=23$ in $^{35}Cl+^{12}C$ at 43 MeV/nucleon (top), $\Sigma Z>23$ in $^{35}Cl+^{24}Mg$ at 43 MeV/nucleon (middle), and $15\leq\Sigma Z\leq 20$ in $^{35}Cl+^{197}Au$ at 43 MeV/nucleon (bottom). Arrows indicate the beam and c.m. velocity for the reverse kinematics system and the projectile velocity for $^{35}Cl+^{197}Au$.

FIG. 3. Θ_{flow} distribution for the $^{35}Cl+^{12}C$ and $^{35}Cl+^{24}Mg$ systems at 43 MeV/nucleon (full line). Dotted and dashed lines are respectively from filtered 1- and 2-source EUGENE simulations respectively.

FIG. 4. Galilean invariant of Z=3 fragments from the $^{35}Cl+^{12}C$ at 43 MeV/nucleon system plotted as a function of perpendicular versus parallel velocity in the c.m. frame with cuts on Θ_{flow} >65° (top panels) and Θ_{flow} <65° (bottom panels). Parallel velocities are along the beam axis (left) and the major axis of the momentum tensor (right). The count yield is in a logarithmic scale.

FIG. 5. Same as fig. 4 but for the $^{35}Cl+^{24}Mg$ at 43 MeV/nucleon with the following cuts on the flow angle: Θ_{flow} >50° (top panels) and Θ_{flow} <50° (bottom panels).

FIG. 6. Anisotropy ratio for $^{35}Cl+^{12}C$ and $^{35}Cl+^{24}Mg$ (full line) and EUGENE 1- and 2-source simulations (dotted and dashed line respectively) with no selection on flow angle.

FIG. 7. Galilean invariant of Z=1 and 2 particles from $^{35}Cl+^{12}C$ (top panels) and $^{35}Cl+^{24}Mg$ (bottom panels) at 43 MeV/nucleon, plotted as a function of perpendicular versus parallel velocities. Parallel velocities are along the beam axis (left panels) and along the momentum tensor's major axis (right panels). The count yield is in a logarithmic scale.

FIG. 8. Galilean invariant of fragments with Z=4,5,6 for the $^{35}Cl+^{12}C$ at 43 MeV/nucleon system with Θ_{flow} <30° (top) and $^{35}Cl+^{12}C$ at 43 MeV/nucleon system with Θ_{flow} <30°(bottom) plotted as a function of perpendicular versus parallel velocity in the c.m. frame. Parallel velocities are along the beam axis (left) and the major axis of the momentum tensor (right). The count yield is in a logarithmic scale.

FIG. 9. Galilean invariant perpendicular versus parallel velocity of IMF ($3 \leq Z \leq 9$) in the c.m. frame for the $^{35}Cl+^{12}C$ at 43 MeV/nucleon system with Θ_{flow} <45° for the heaviest (top left) and second heaviest (top right) ions detected in the phoswich detectors and heaviest ions detected in the CsI(Tl) scintillators (bottom left) and total of the three distributions (bottom right). Orientation is relative to the major axis of the momentum tensor. The count yield is in a logarithmic scale.

FIG. 10. Same as figure 9 but for EUGENE 2-source $^{35}Cl+^{12}C$ at 43 MeV/nucleon simulations with b> 4.0 fm, with Θ_{flow} <45°.

FIG. 11. Same as figure 9 but for the $^{35}Cl+^{24}Mg$ system at 43 MeV/nucleon with Θ_{flow} <30°. The heaviest and second-heaviest forward fragment may also have been detected in the Si-Csi small-angle telescopes.

FIG. 12. Same as figure 11 but for EUGENE 2-source $^{35}Cl+^{24}Mg$ at 43 MeV/nucleon simulations with b> 3.8 fm, with Θ_{flow} <30°.

FIG. 13. Parallel velocity of Z=1 (top left), 2 (top right), 3 (bottom left) and 4 (bottom right) from the $^{35}Cl+^{197}Au$ system at 43 MeV/nucleon with ΣZ (detected)>15. Full lines are for data, dashed line for 2-source GENEVE simulations.

FIG. 14. Parallel velocity of Z=1 from the PLE (dashed, top panel), TLE (dashed, middle panel) and preequilibrium emission (dashed, bottom panel) compared to the total distribution (full line) predicted by 2-source GENEVE simulations.

FIG. 15. Ratio of protons (mass=1), deuterons (mass=2) and tritons (mass=3) to the respective total number of hydrogens emitted forward of 4 cm/ns and backward of -4 cm/ns (see text for details). Data are represented by full dots for forward emission and empty dots for backward emission and the GENEVE simulation by a full line for forward emission and a dashed line for backward emission.

FIG. 16. Time evolution of density profiles on the reaction plane for $^{35}Cl+^{12}C$ at 43 MeV/nucleon reaction, at three impact parameters calculated with the BUU model (unfiltered).

FIG. 17. The mass distribution for pre-fragment emission, plotted against impact parameter b for $^{35}Cl+^{12}C$ at 43 MeV/nucleon reaction at t=120 fm/c with QMD calculation (unfiltered). Each contour represents a factor slightly higher than 2.

FIG. 18. Unfiltered QMD calculation of the differential cross section $d\sigma/db$ for the production of one, two, and three IMF plotted against impact parameters b for the $^{35}Cl+^{12}C$ reaction at 43 MeV/nucleon at t=120 fm/c. The full line represents the impact parameters distribution used in the simulation.

FIG. 19. Unfiltered QMD calculation of the IMF velocity components (v_z) versus position components z on the beam direction (z axis) for three-IMF events in the $^{35}Cl+^{12}C$ reaction at 43 MeV/nucleon at t=120 fm/c.

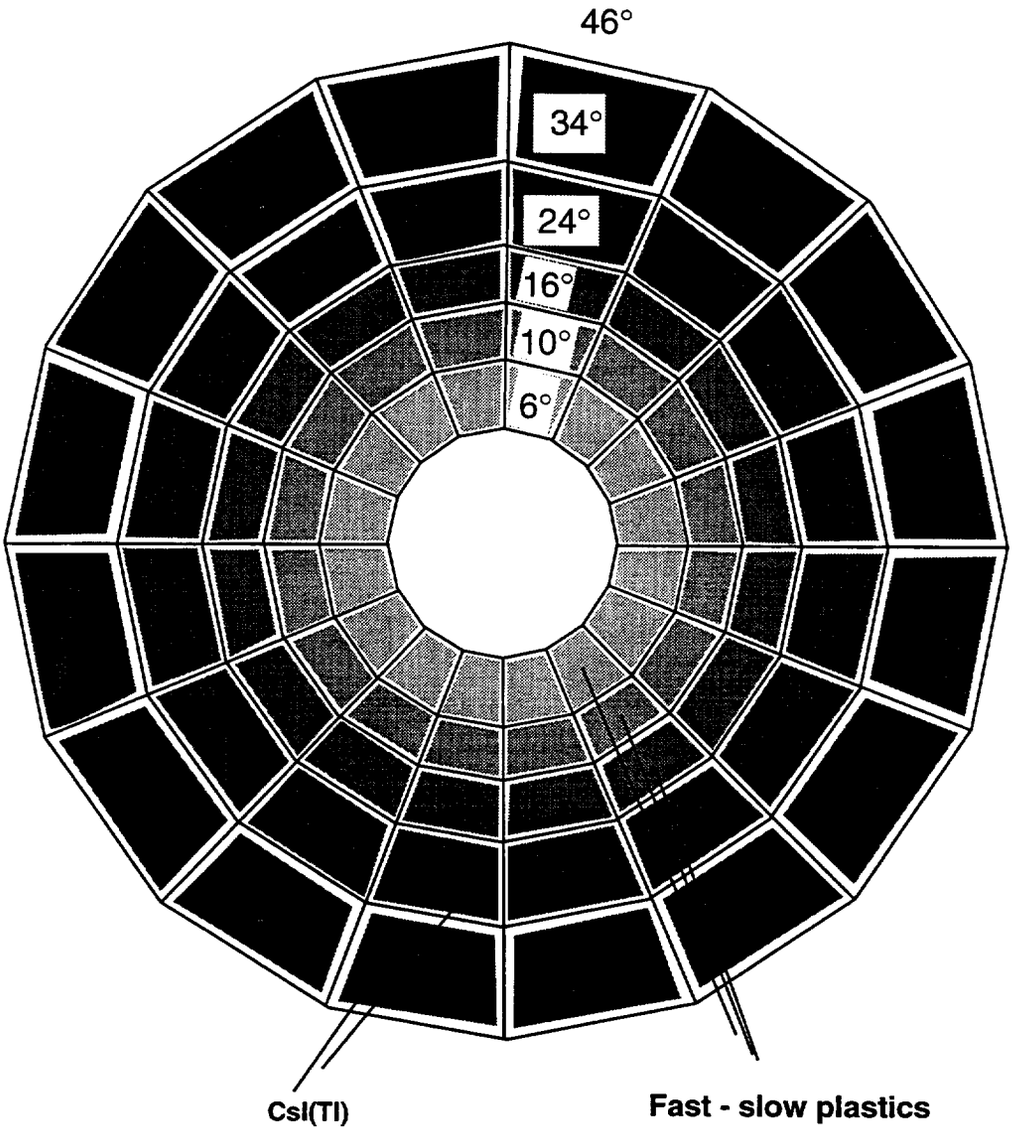

FIG. 1. Y.Larochelle et al.

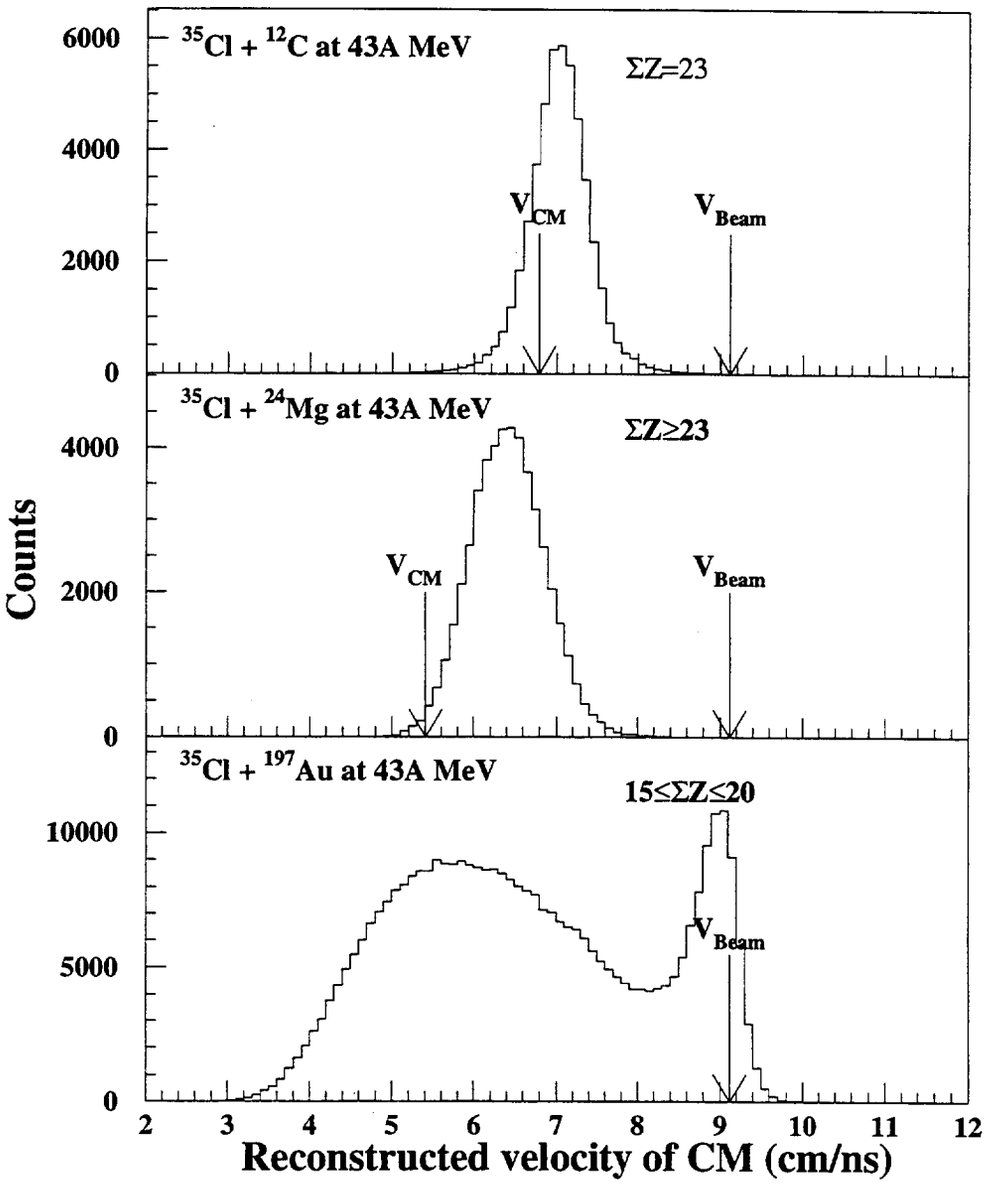

FIG. 2. Y.Larochelle et al.

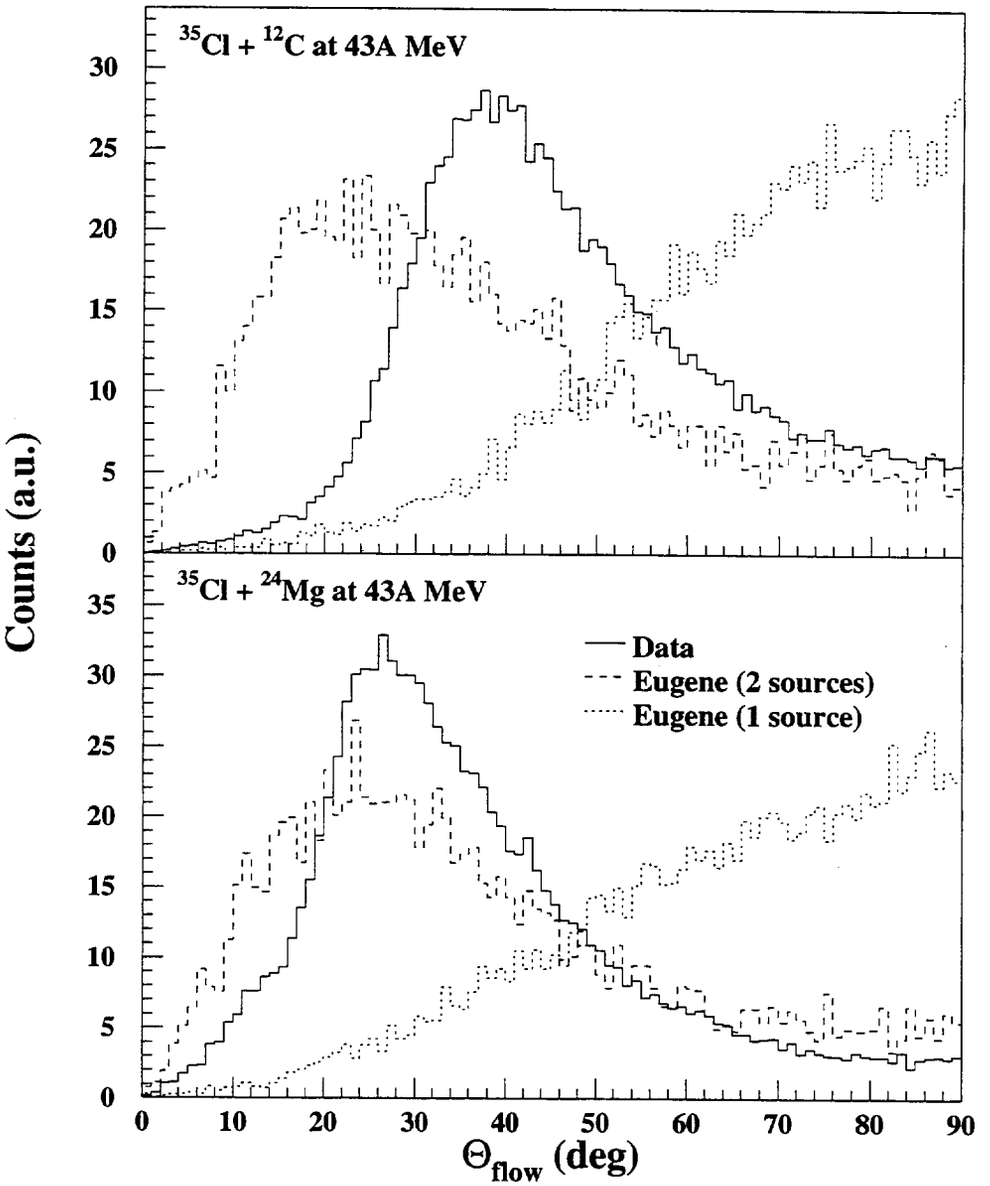

FIG. 3. Y.Larochelle et al.

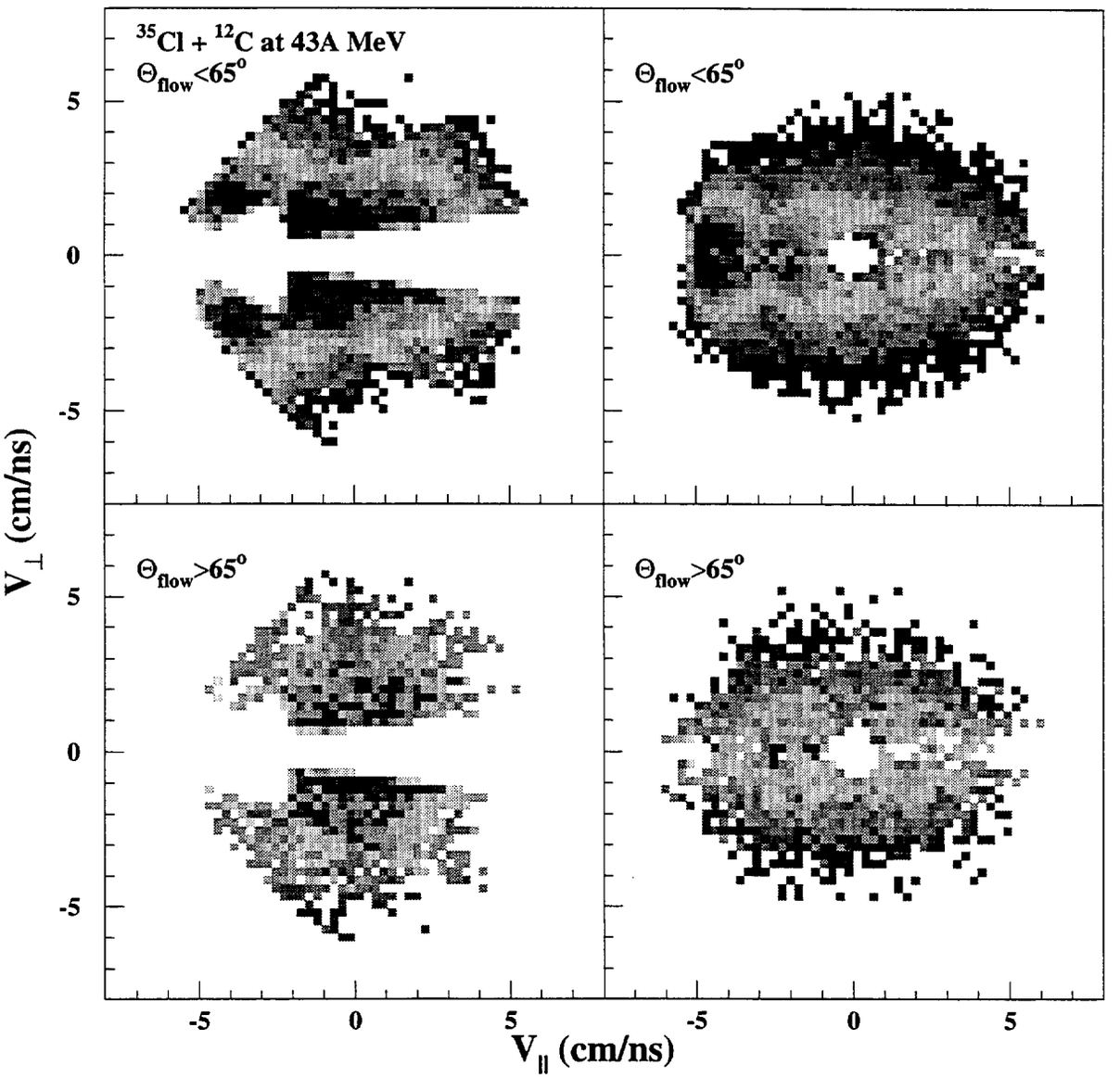

FIG. 4. Y.Larochelle et al.

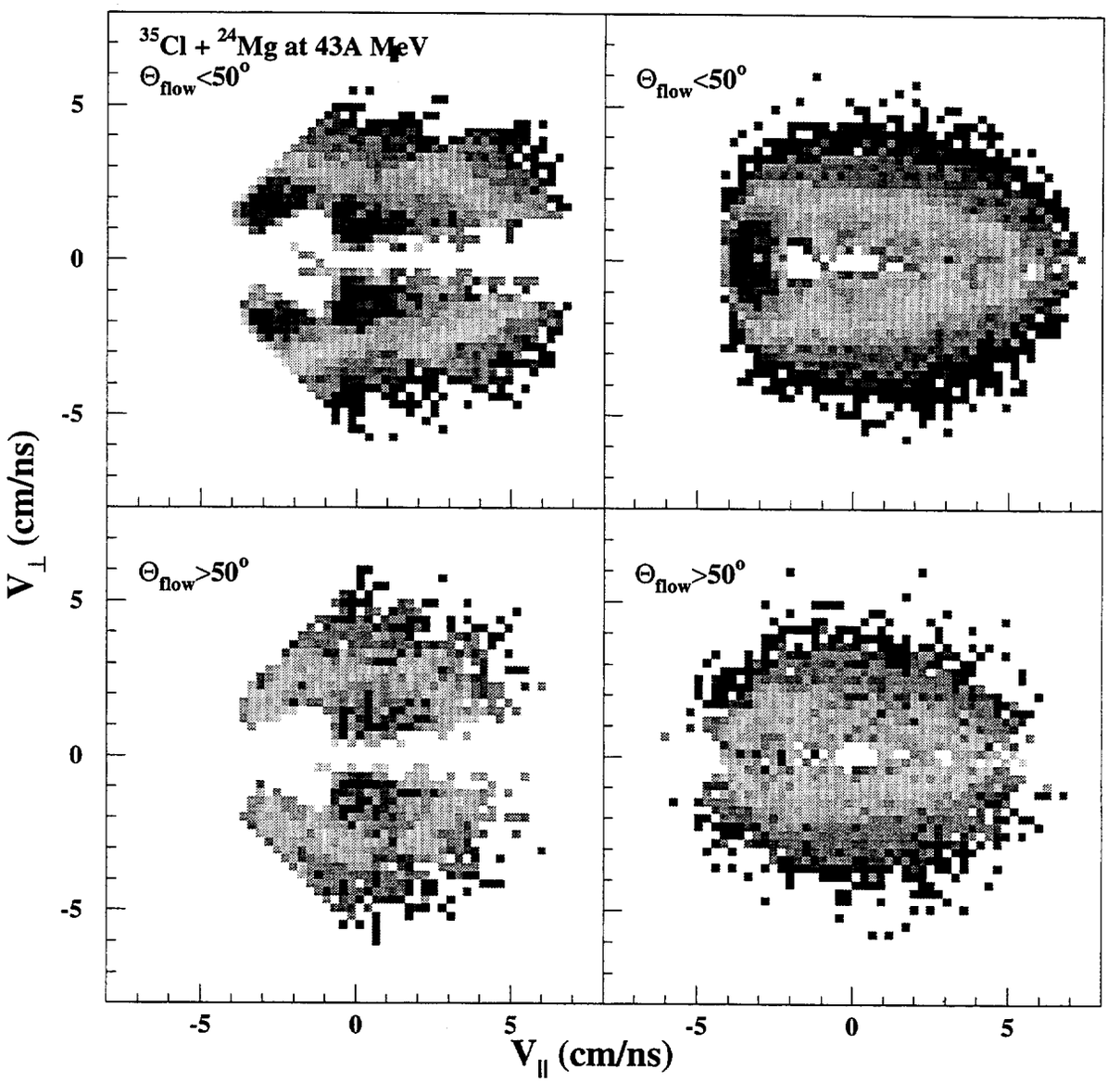

FIG. 5. Y.Larochelle et al.

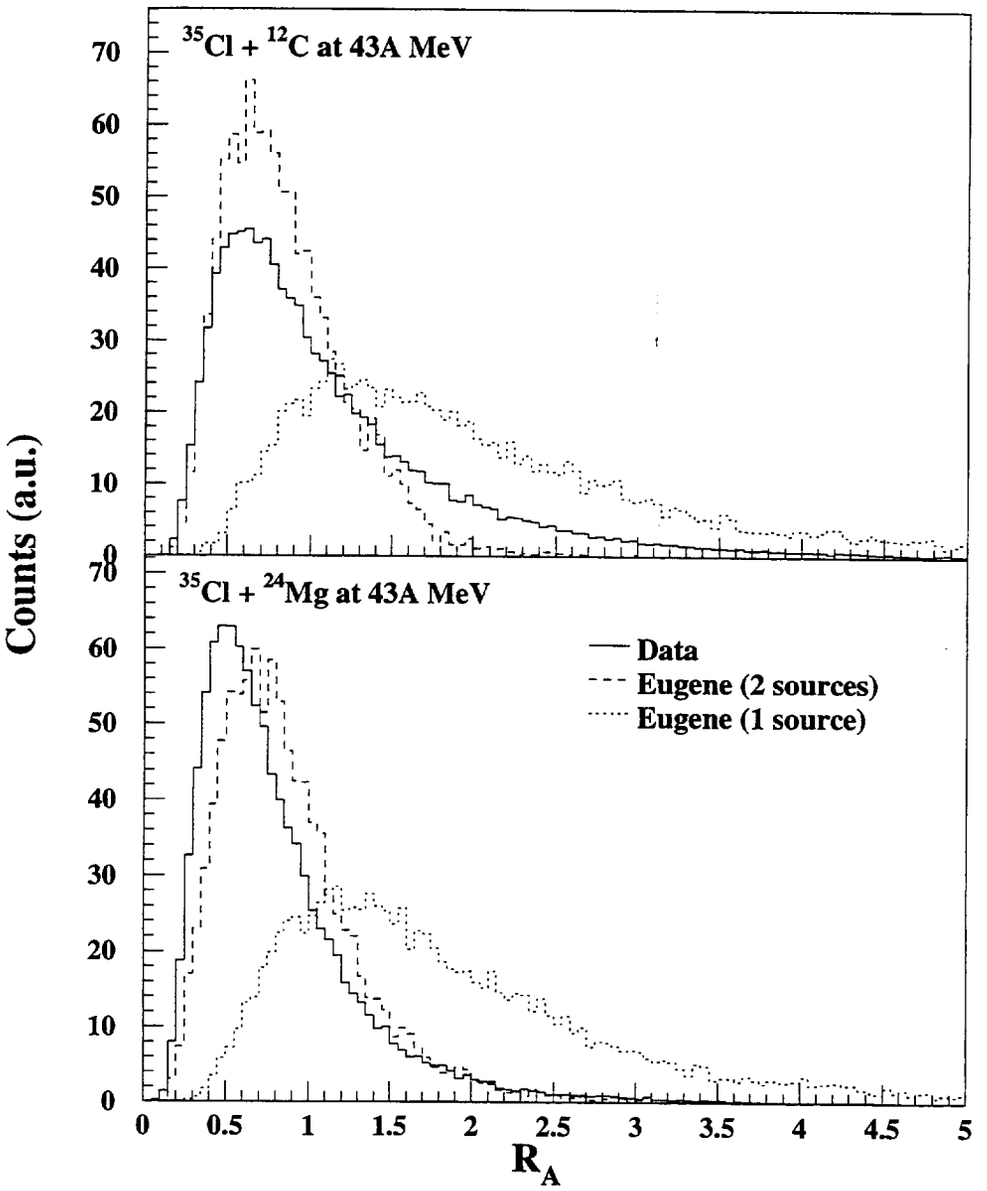

FIG. 6. Y.Larochelle et al.

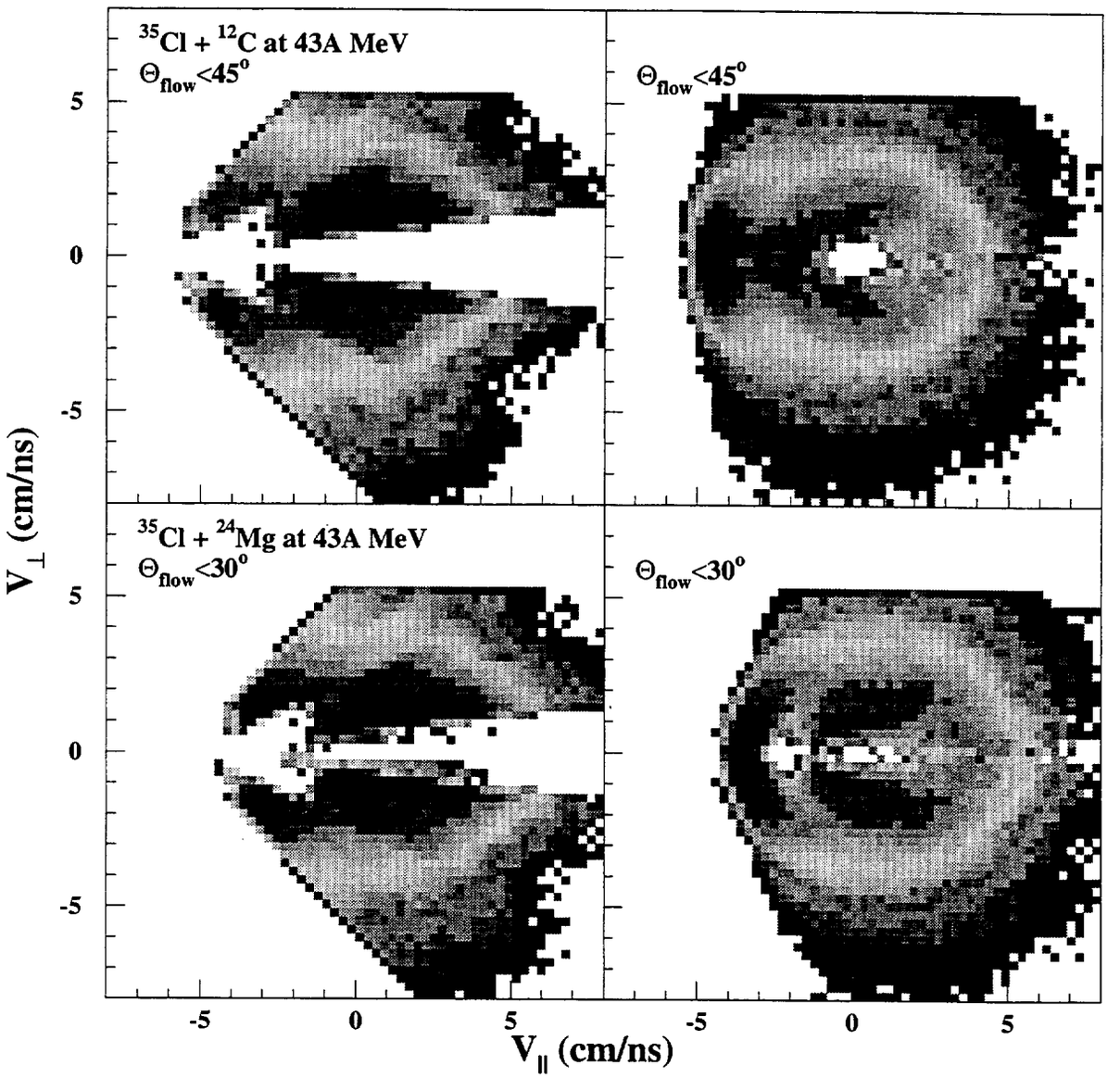

FIG. 7. Y.Larochelle et al.

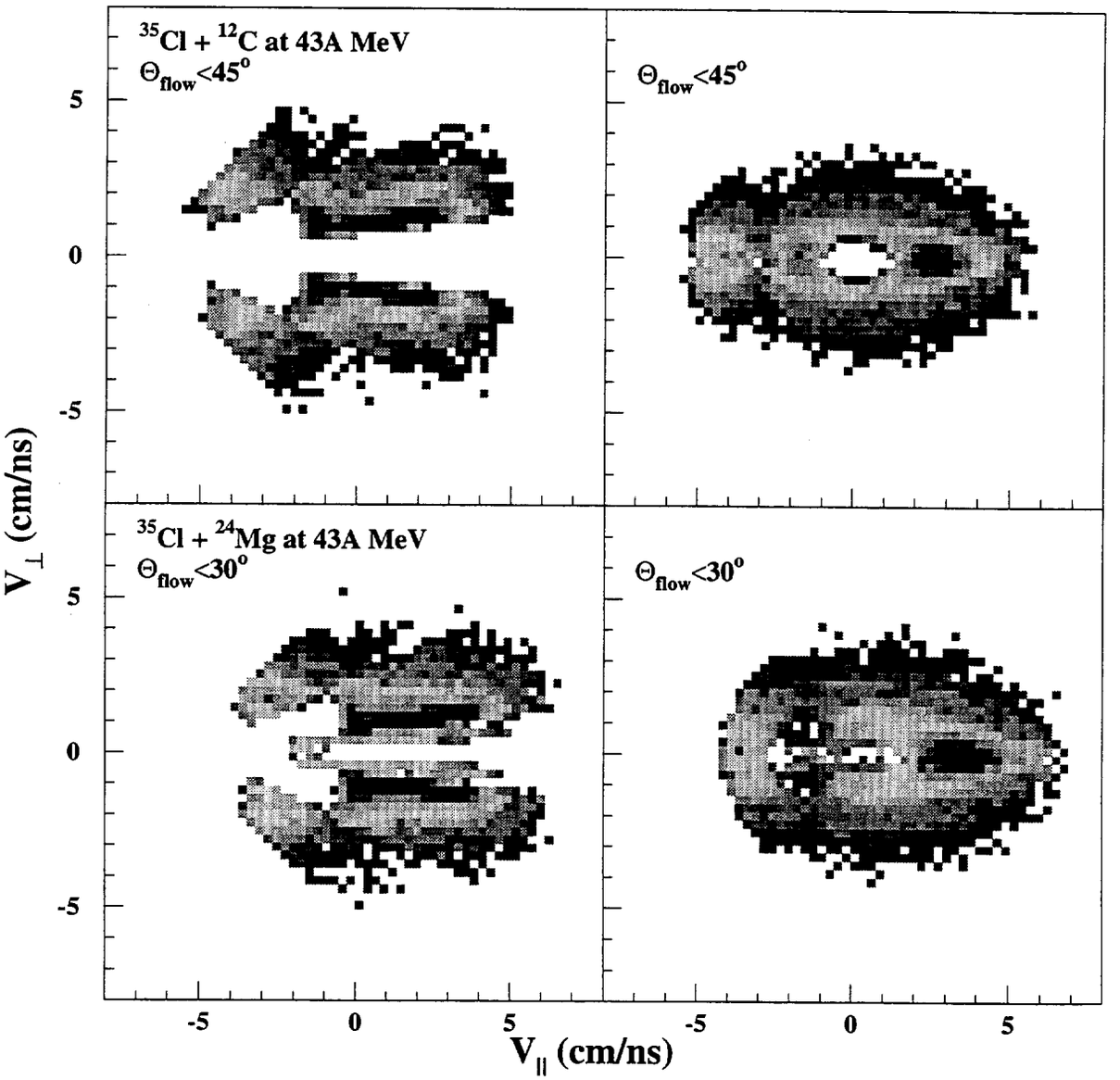

FIG. 8. Y.Larochelle et al.

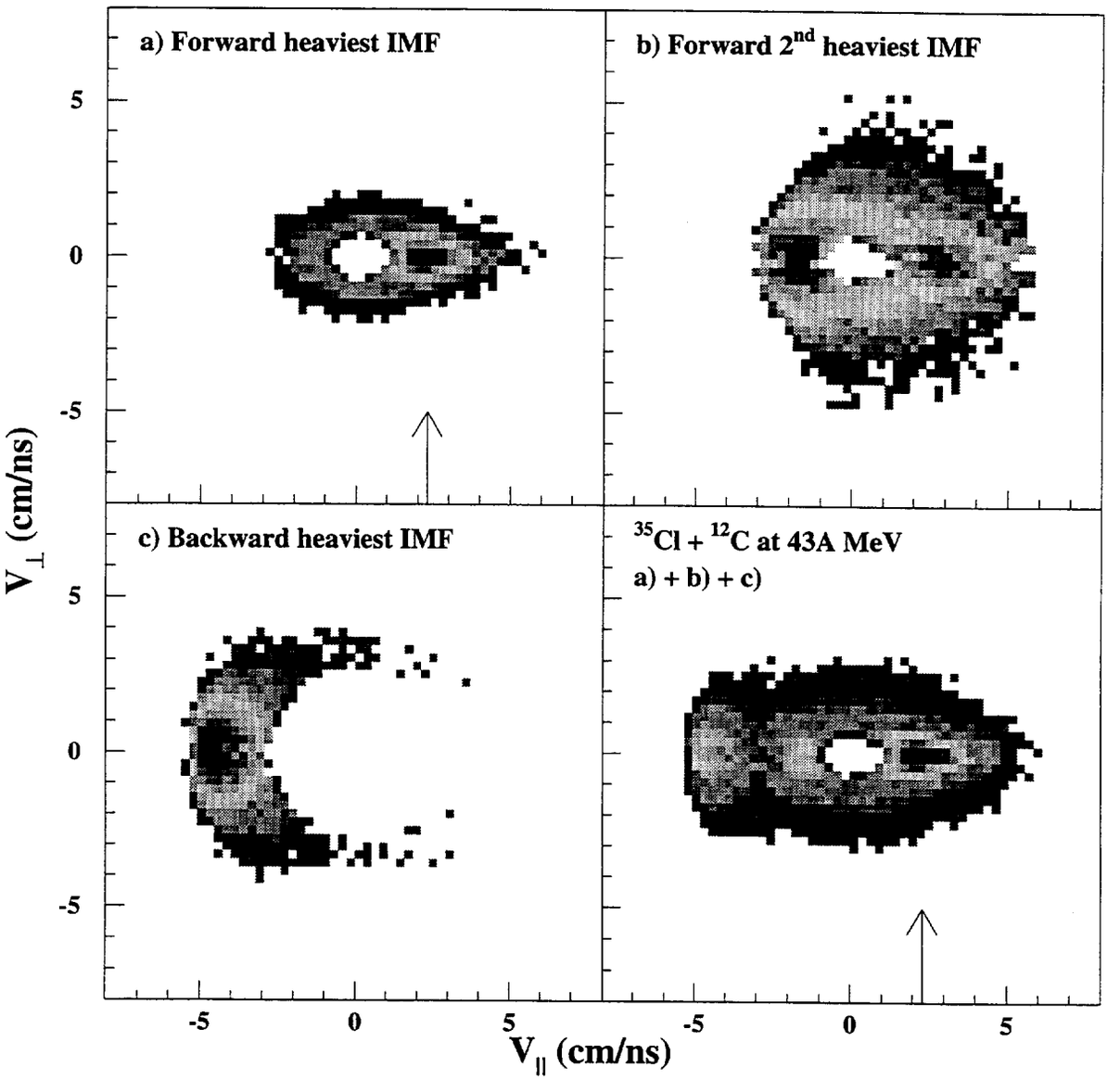

FIG. 9. Y.Larochelle et al.

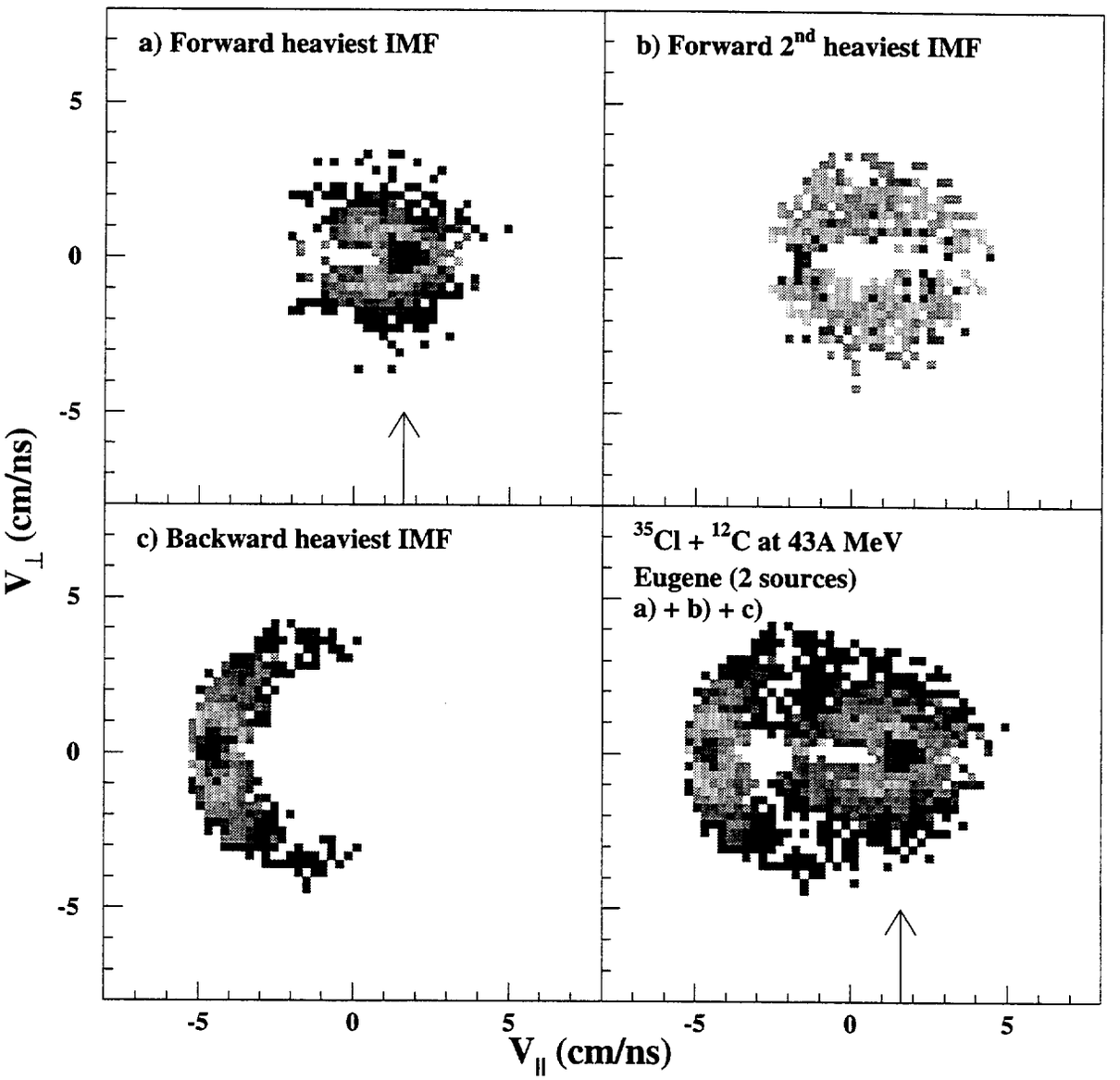

FIG. 10. Y.Larochelle et al.

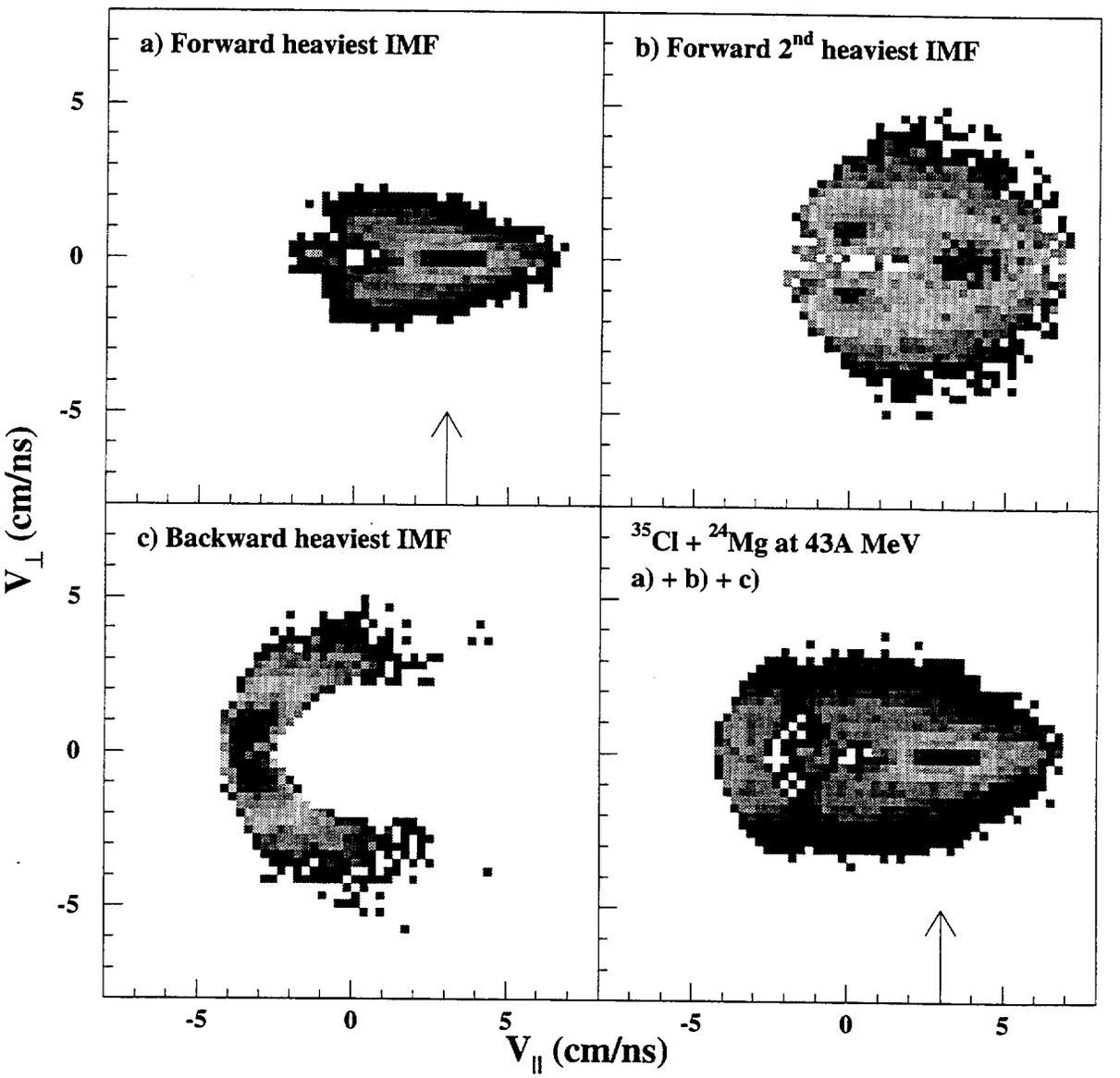

FIG. 11. Y.Larochelle et al.

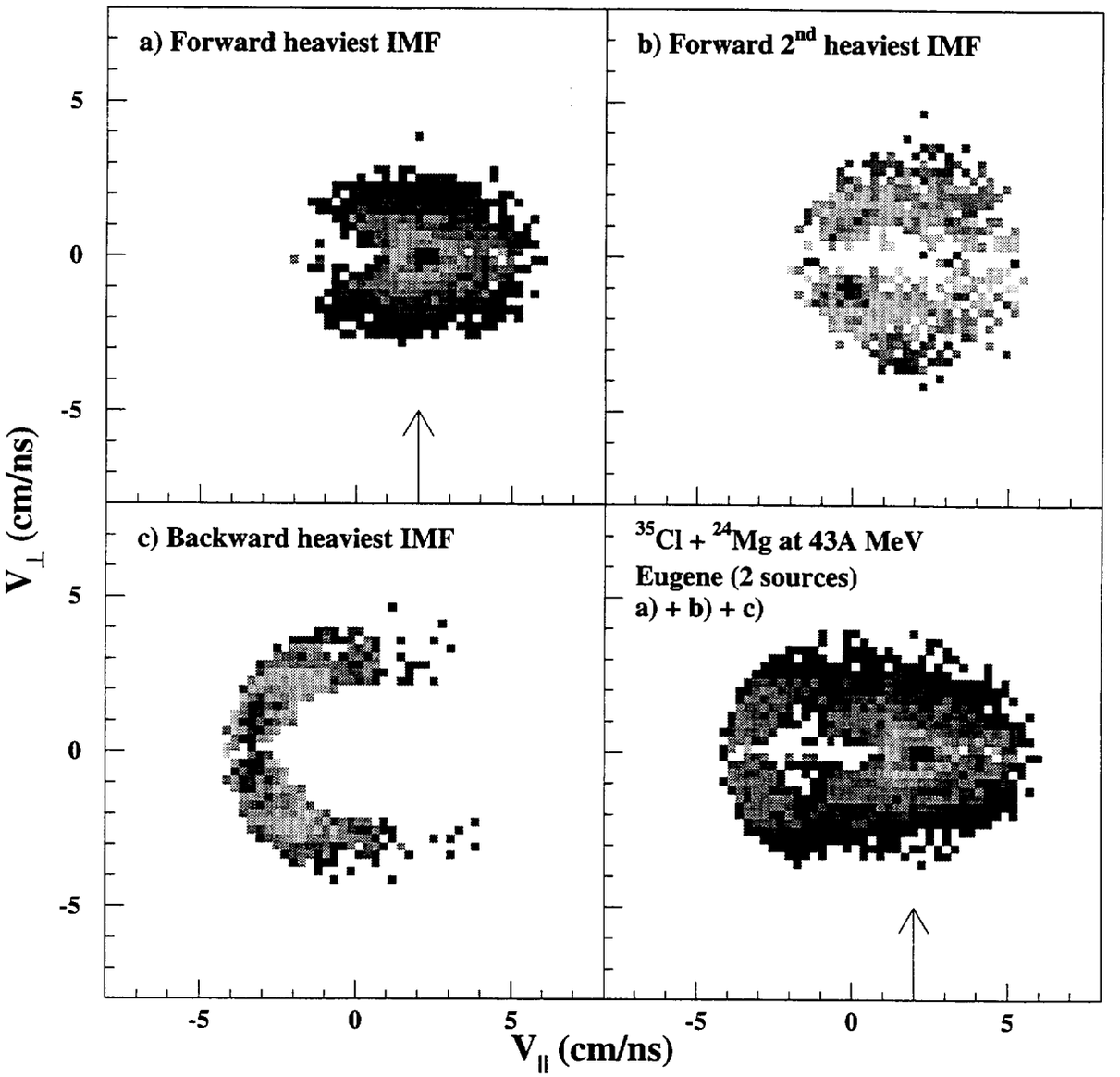

FIG. 12. Y.Larochelle et al.

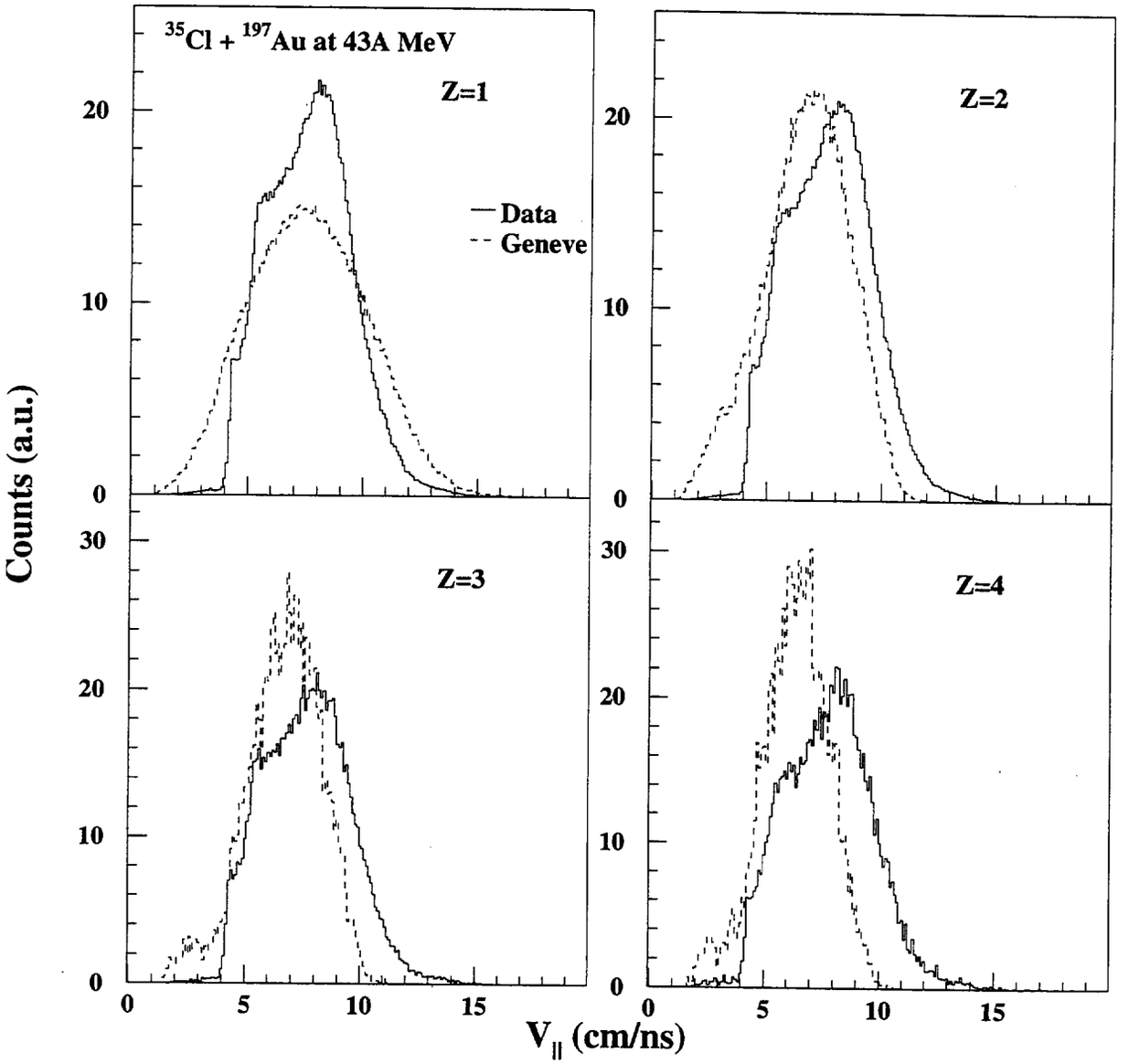

FIG. 13. Y.Larochelle et al.

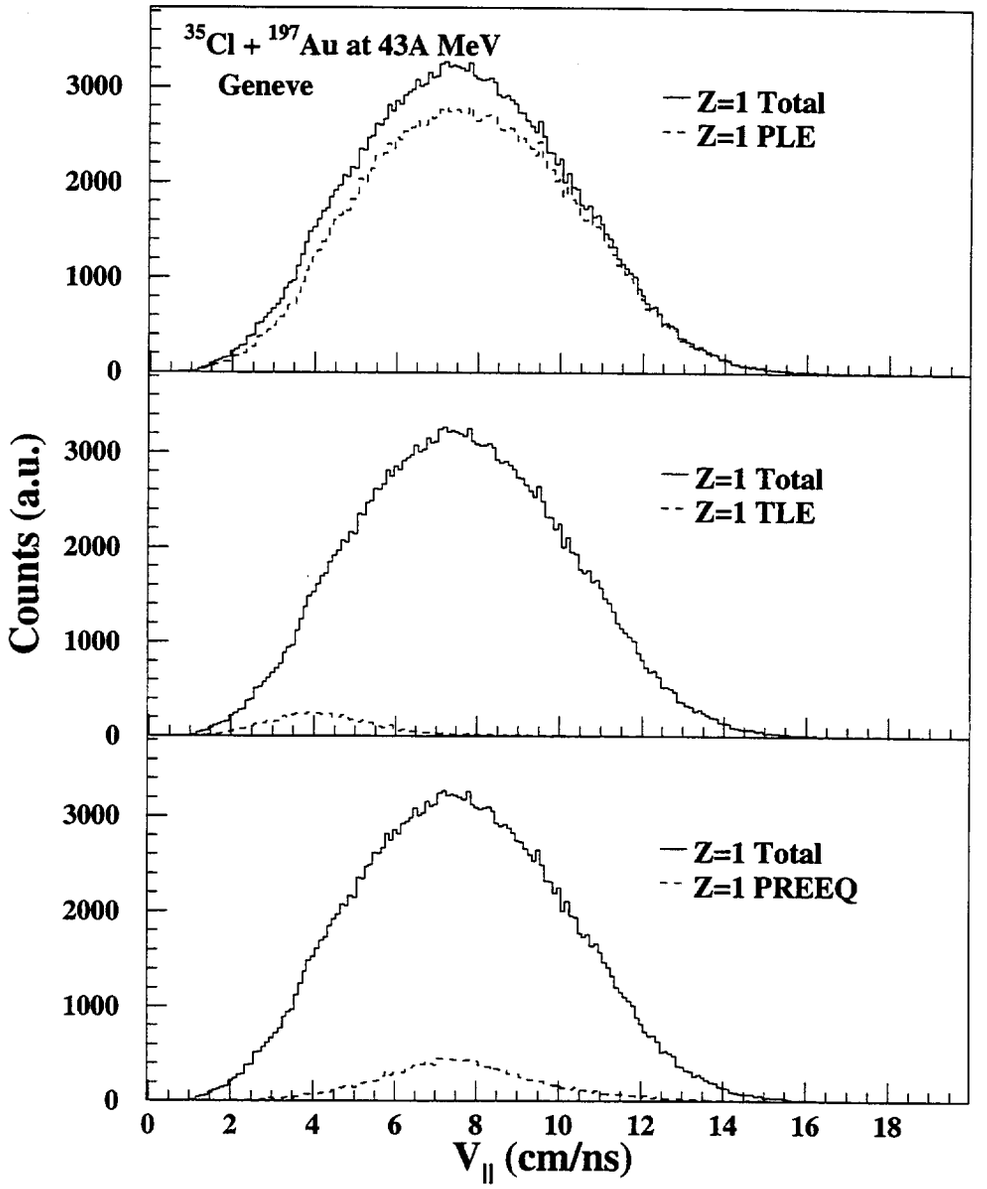

FIG. 14. Y.Larochelle et al.

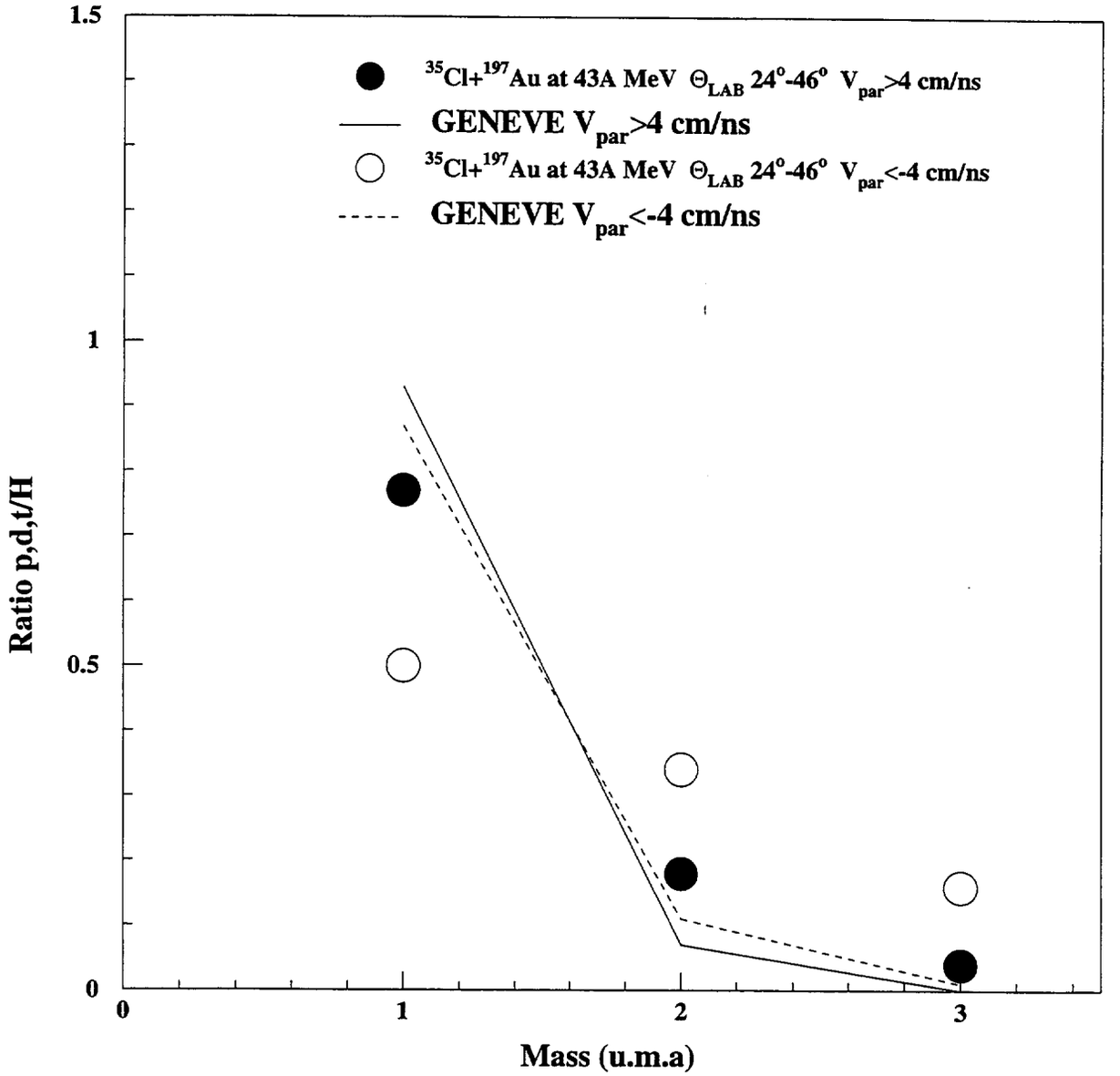

FIG. 15. Y.Larochelle et al.

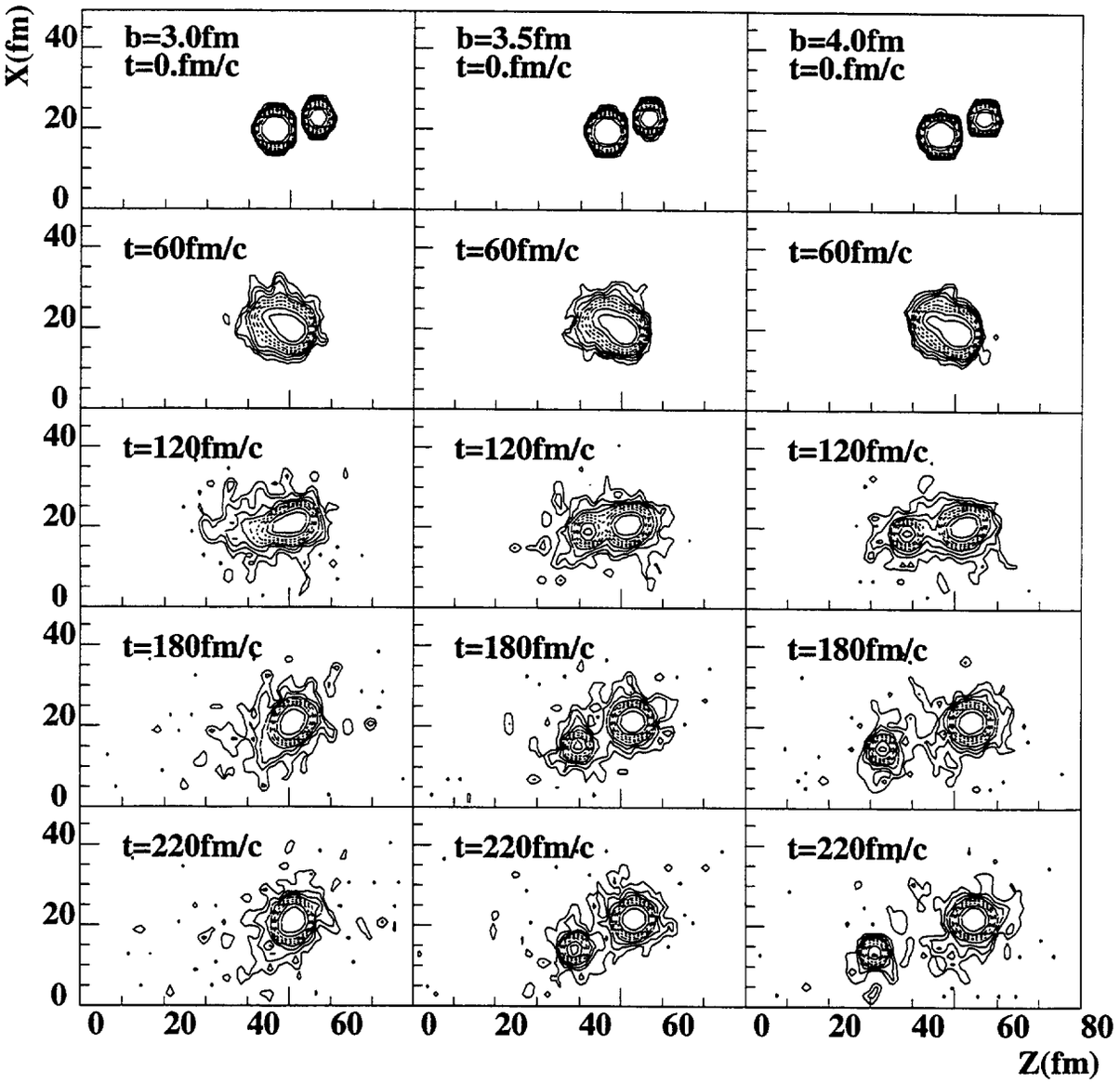

FIG. 16. Y.Larochelle et al.

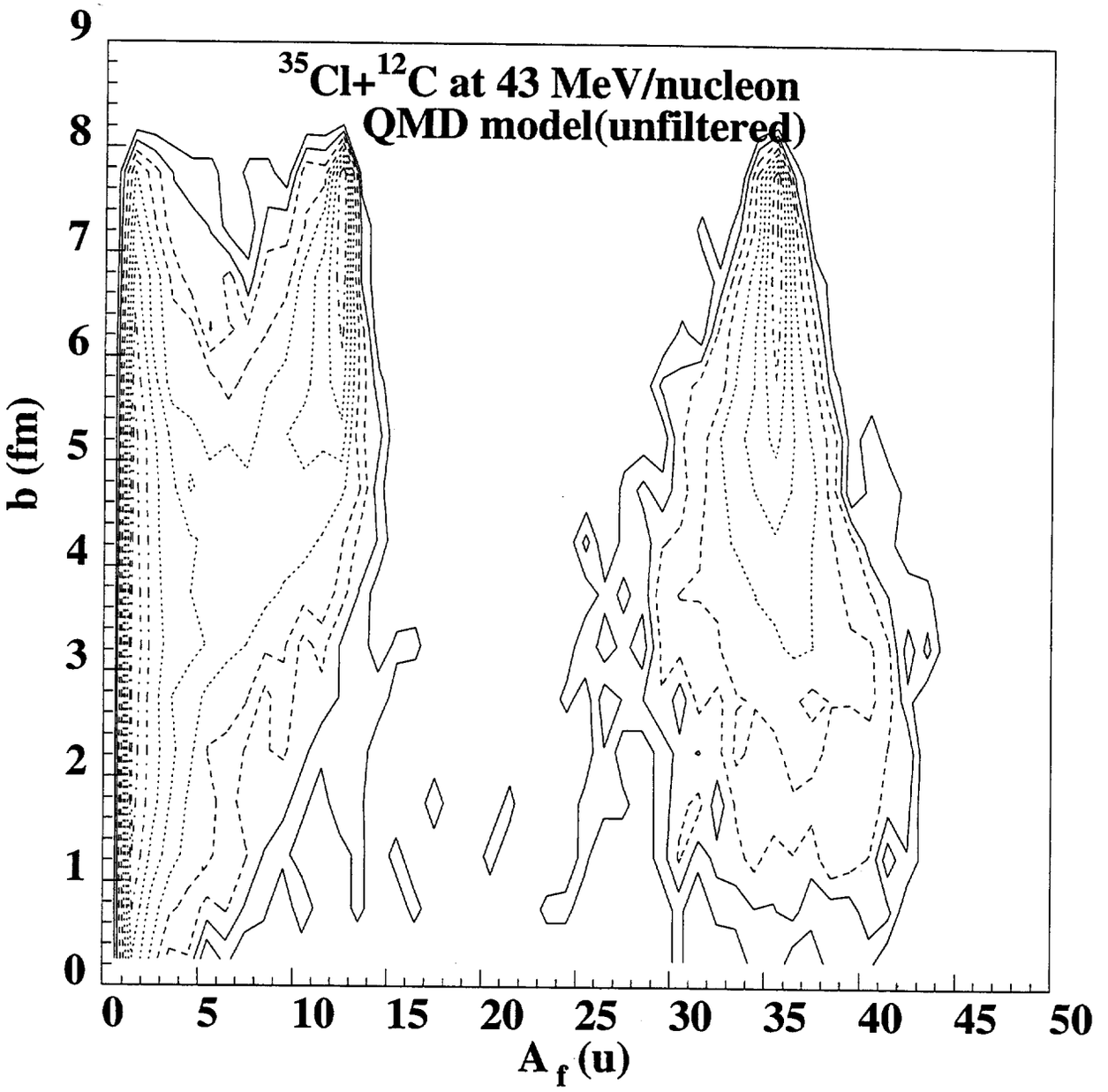

FIG. 17. Y.Larochelle et al.

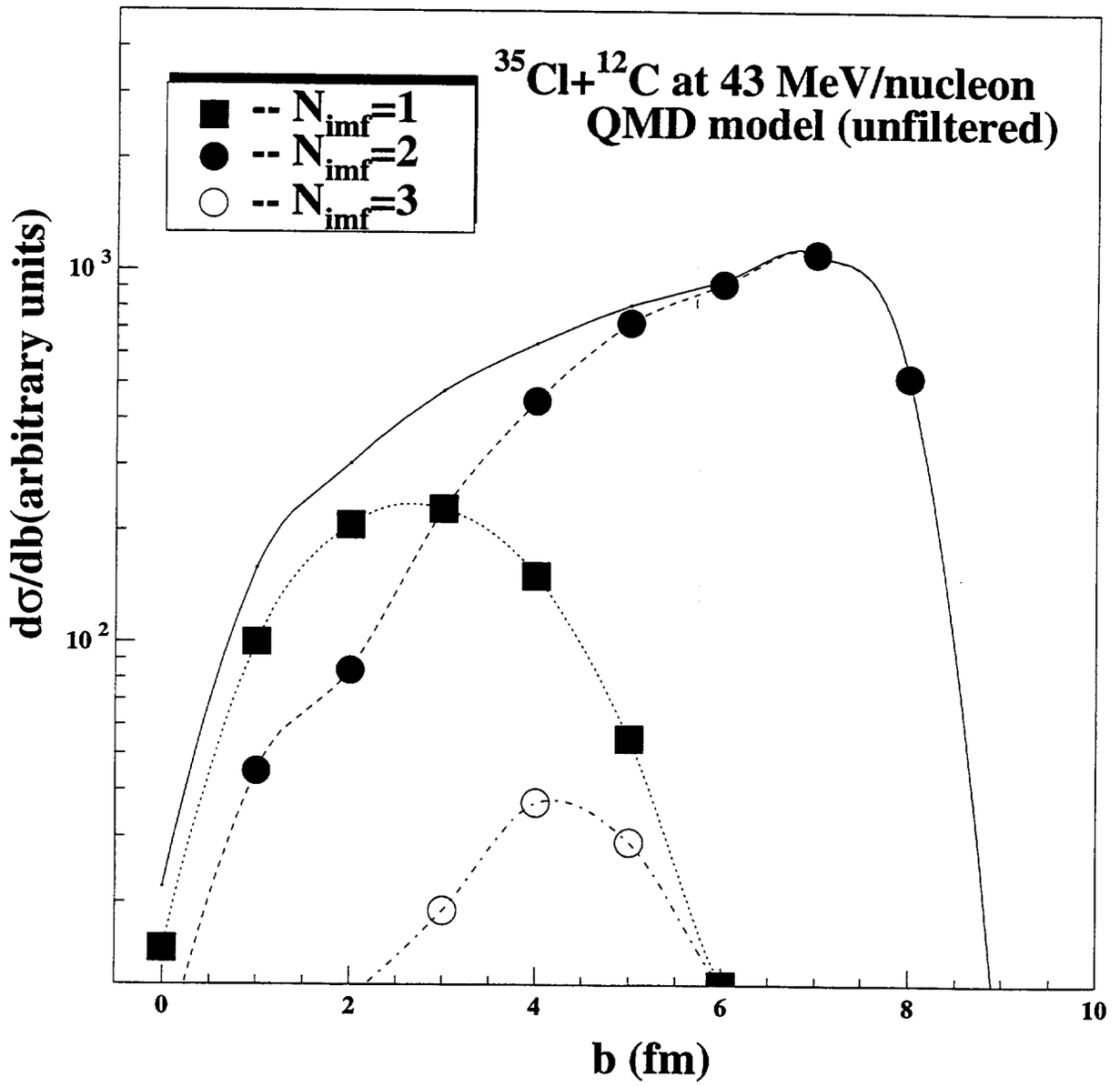

FIG. 18. Y.Larochelle et al.

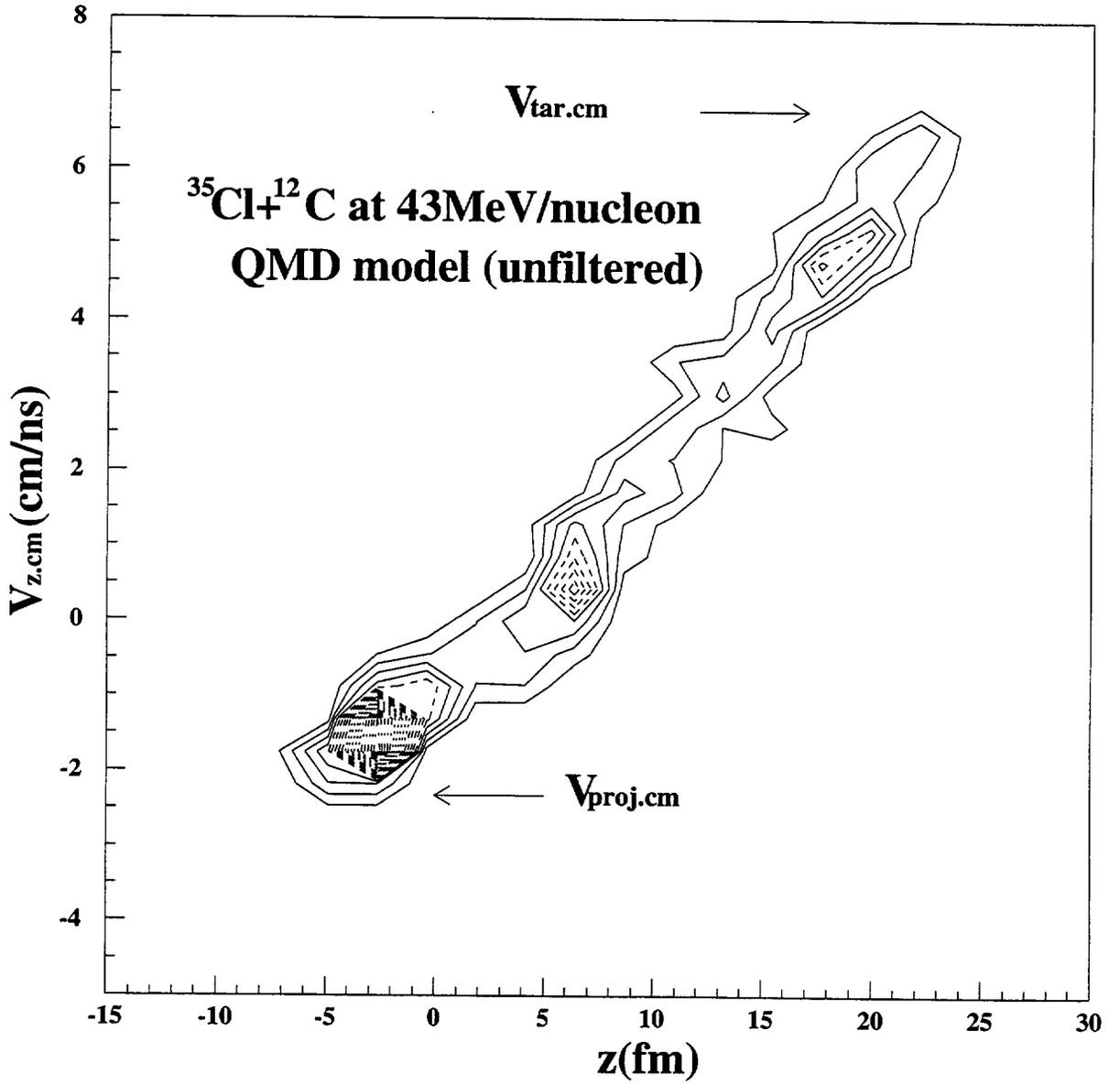

FIG. 19. Y.Larochelle et al.